RICE UNIVERSITY

An All Solid-State Laser System for Trapping Lithium

by

Melissa C. Revelle

A Thesis Submitted
in Partial Fulfillment of the
Requirements for the Degree

Masters of Science

Approved, Thesis Committee:

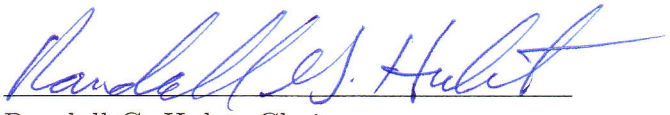

Randall G. Hulet, Chair
Fayez Sarom Professor of Physics and Astronomy

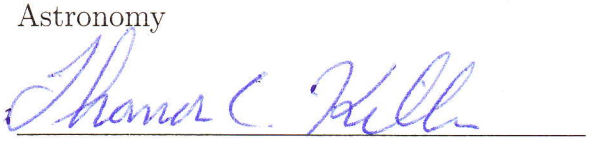

Thomas. C. Killian
Professor of Physics and Astronomy

Emilia Morosan
Assistant Professor in Physics and Astronomy

Houston, Texas

April, 2013

Abstract

An All Solid-State Laser System for Cooling and Trapping Lithium

by

Melissa C. Revelle

Ultra-cold atoms have become an essential tool in studying phenomena in condensed matter systems such as superconductivity and quantum phase transitions. To study fermions in one-dimension we use an apparatus built to trap and cool lithium atoms down to nano-Kelvin temperatures. Recently, significant upgrades to the laser system have been made to improve performance, increase stability, minimize maintenance and improve flexibility. We are working towards two exciting projects: proving the existence of an exotic superfluid state (FFLO) and probing the crossover between one and three-dimensions in a spin-$\frac{1}{2}$ Fermi gas with a spin-imbalance.

Contents

Illustrations

Tables

Chapter 1

Introduction

The main chamber of the apparatus has been under vacuum for nearly 15 years. In that time, the physics we study has evolved from the optimization of dual evaporation in the magnetic trap [1] to the creation of a spin-imbalanced Fermi gas in one and three-dimensions [2–4].

Since the last review of the apparatus [2, 5] there have been many significant changes to the laser system. This will serve primarily as a guide to the portions of the experiment that have changed, with a focus on the laser system. I will begin with a brief introduction to the apparatus to give a clear picture of our motivations.

1.1 Overview

We have studied many interesting phenomena that have lead us in the direction of our current projects. After the proof of pairing in balanced systems [6], it was noticed that in 3D imbalanced systems, multiple phases exist and separate from one another [7]. Originally, we created a metastable state by evaporating too forcefully in our single-beam trap [8, 9]. The temperature of the atoms was comparable to the trap depth during evaporation, and due to the configuration of our trap, there was preferential evaporation from the center of the trap [9]. While the gas was phase separated, the geometry was quasi-1D, causing the separation to form in the wings instead of in 3D shells.

The next project involved a full study of the 1D phase diagram (Fig. 1.1) for a spin-imbalanced Fermi gas by confining the gas to a 2D array of 1D tubes [3, 4, 10]. This spurred many questions we must now endeavour to answer. In 1D, the center

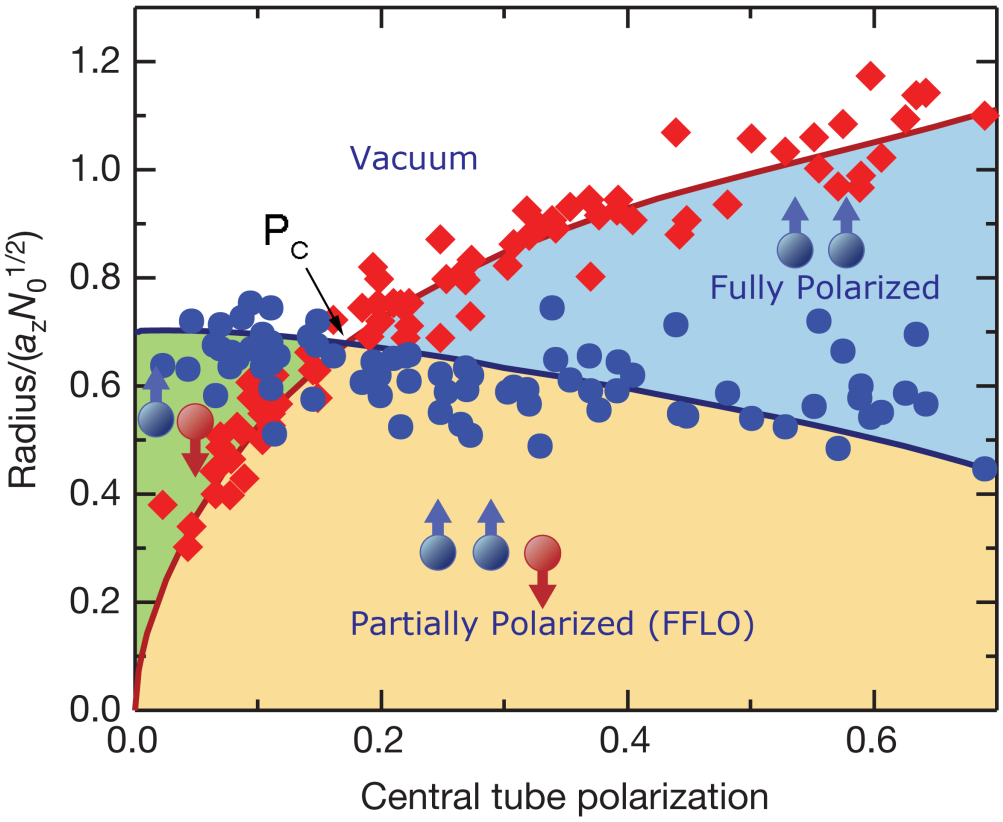

Figure 1.1 : The Experimental 1D Phase Diagram [4]. The scaled radius of the axial density difference (red diamonds) and the minority state (blue circles) are compared to 175 nK Bethe ansatz theory (solid lines). The partially-polarized phase is present at the center of the tubes for all polarizations while the wings change from fully-paired to fully-polarized at a polarization of $P = 0.13 \pm 0.03$.

of the tubes are occupied by a partially-polarized phase and the wings are either fully-paired or fully-polarized depending on the polarization. This is inverted from in 3D. Additionally, it is suggested that the partially-polarized phase is an exotic superfluid phase (FFLO) that has yet to be experimentally characterized. This lead to two interesting avenues of pursuit.

1.1.1 The 1D-3D Crossover

The phase diagram in 1D is inverted from that in 3D [11, 13]. As mentioned before, in 1D, the partially-polarized phase is in the center of the tubes. But in 3D, Fig. 1.2

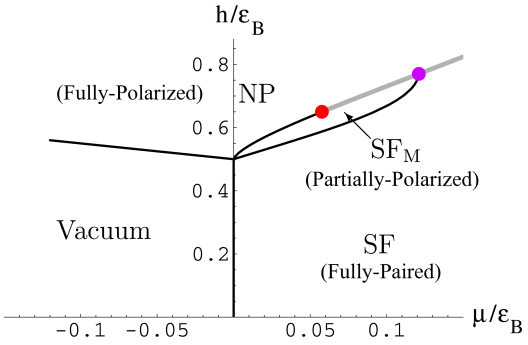

Figure 1.2 : Theoretical 3D phase diagram in the Bose-Einstein Condensate (BEC) regime, where the scattering length is positive (adapted from [11]). The axes are the chemical potential, μ, which corresponds to the radius of the cloud and the effective magnetic field, h, which is the spin polarization where $h = 0$ gives equal spin mixures. Both axes are normalized to the molecular binding energy, ϵ_b. The center of the cloud is at large values of μ/ϵ_b for which most values of the polarization have a superfluid (SF) core. In a trap, the polarization is fixed, but the chemical potential will vary from the center to the edge. There is a region of polarized superfluid (SF_M, different from FFLO) between the SF and the normal fully-polarized (NP) phase but this occupies a very small region of the phase diagram as compared to either the 1D or the crossover regime.

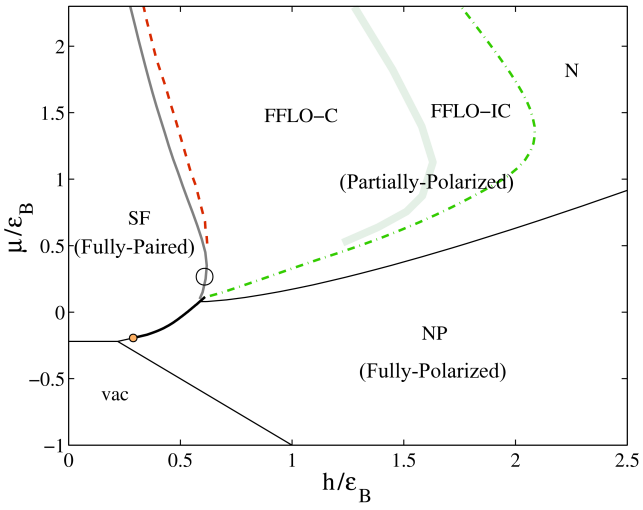

Figure 1.3 : Theoretical phase diagram of the 1D-3D crossover (adapted from [12]). This is for a fixed lattice depth in the crossover regime with each axis scaled to the binding energy, ϵ_B, to make them dimensionless. Small chemical potential, μ/ϵ_B, is more toward the edge of the cloud where the lattice filling is low. The other axis is polarization (h/ϵ_B), which is constant within the cloud. For most polarizations the cloud has a mixture of 3D and 1D structure. The core of the cloud consists of the FFLO phase but there are more than two phases present for most polarizations. N represents a partially-polarized normal liquid, SF is a superfluid phase and NP is a fully-polarized phase.

shows the fully-paired phase occupies the core of the cloud [7,14]. In our experiment, we can easily study the crossover regime, where the lattice depth is too small to be considered 1D because there is still strong coupling between the tubes. By slowly increasing our lattice depth from a 3D trap configuration, we can map out a phase diagram though the crossover from 3D to 1D similar to Fig. 1.3.

In the crossover regime, a single tube can exhibit both 1D and 3D properties. It is expected that for most polarizations the core will consist of the partially-polarized phase as in 1D, but there will be multiple shells, such as a superfluid middle shell surrounded by a normal polarized phase as in 3D [12]. Additionally, the quasi-1D phase diagram may help find the ideal polarization and lattice strength for conclusive proof of FFLO, if the partially polarized FFLO phase still occupies a large portion of the phase diagram, but this will be discussed in Sec. 1.1.2.

1.1.2 The Exotic Fulde-Ferrell-Larkin-Ovchinnikov Phase

In 1964, an exotic superfluid phase, Fulde-Ferrell-Larkin-Ovchinnikov (FFLO), was predicted to exist in magnetized superconductors [15, 16]. It is suggested that FFLO is a superfluid state that pairs under a magnetic field, or in the case of cold atoms, in a spin-imbalanced system which is analogous to an applied magnetic field. Due to the unequal Fermi momenta, the resulting pairs then have a non-zero center of mass momentum. The unpaired atoms remain mixed with the paired atoms in a way that creates an oscillating superfluid order parameter [17, 18] and spin density fluctuations [19]. The 1D phase diagram (Fig. 1.1) is well described by Bethe ansatz theory which suggests that the partially-polarized phase is the exotic FFLO [4]. This phase diagram shows that a large range of polarizations will result in an FFLO phase. In 3D, FFLO only exists as a small sliver on the phase diagram far from the Feshbach resonance with negative scattering length [20] (it does not appear on Fig. 1.2). Since

the FFLO phase exists in a larger region of the 1D phase diagram and cloud, this is the regime that we will conduct our experiment.

As of yet, there has been no conclusive proof for the existence of FFLO, but there have been many suggestions on how to make a definitive observation by interference [18, 21] and spectroscopy [17, 19]. Each method is promising in its own way, but direct observation of the pair momentum distribution via time of flight expansion in 1D is the most suitable for our experiment [22, 23]. This is because it involves few experimental modifications (discussed in Sec 6.3.2) and has a distinctive feature that should be easily observable even when considering finite temperature effects and the multiple tubes in the system. The expansion must be limited to along the tubes because of the confinement from the lattice. If the atoms were freely released in 3D, the expansion would be faster from the tightly confined directions and would dominate the expansion, in the time needed to see the pair momentum distribution the cloud will dissipate. Since FFLO is formed in 1D, the signature momentum distribution is along the axis of the tubes.

A finite center of mass pair momentum is unique to FFLO and we expect to observe this momentum at:

$$q = \pm|k_F^{\uparrow} - k_F^{\downarrow}|, \tag{1.1}$$

where $k_F^{\uparrow,\downarrow}$ is the Fermi momentum of the majority and minority states. We focus on the pair momentum because the FFLO signature is not observable in the momentum distribution of the unpaired atoms even after release from the lattice, this as shown in Fig. 1.4. Also shown in Fig. 1.4 is the pair momentum distribution, where the signature peaks from FFLO are seen. The FFLO phase occupies the center of the tubes for most polarizations and is prevalent for polarizations (P) near the critical polarization (P_c), therefore, these momentum peaks should be visible. However, they may be more difficult to observe due to finite temperature effects and the multiple

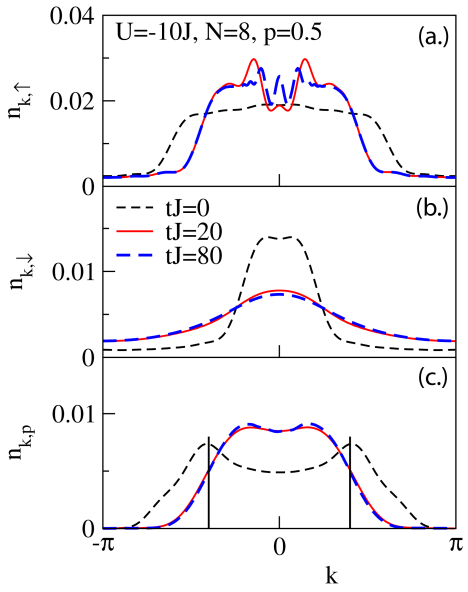

Figure 1.4 : The momentum distribution of the (a) majority atoms and (b) the minority atoms, neither show evidence of FFLO. (c) The pair momentum distribution where the FFLO peaks can be seen. Each plot shows the distribution for different time of flights in the lattice, this shows that even after being released from the trap the momentum distribution in the pairs represents the initial state [23].

tubes. This is why the quasi-1D regime may be best for proving FFLO, there the tubes are slightly coupled which will phase lock the FFLO in each tube and hopefully strengthen the signal [22].

1.2 Apparatus

This apparatus is perhaps the most complicated of the three apparatus in our lab because it requires ^{7}Li for cooling of the fermionic isotope of lithium, ^{6}Li. Identical fermions, such as ^{6}Li in a single spin state, are quantum mechanically forbidden from s-wave collisions with themselves at low temperatures due to the odd symmetry of their wave functions. Therefore, ^{6}Li cannot be used to thermalize with itself during evaporation. Bosons have an even symmetry and can interact with both themselves and fermions, and are used to aid in the cooling of ^{6}Li.

The experiment starts with both isotopes heated to about 400° in an oven to

produce a thermal beam, as described in Gutherie Partridge's Ph.D thesis [2]. The thermal beam is aimed toward a Zeeman slower (design details in Kevin Strecker's MS thesis [1]), which serves to slows atoms using a laser tuned to resonance with the atoms, such that the laser beam imparts momentum opposing the movement of the atoms. The direction of spontaneous emission is random, and thus there will be an overall net loss of forward momentum. The atoms are moving so fast out of the oven, however, that the energy levels are Doppler shifted and as they slow the frequency of the transition changes. This shift can be compensated by using the Zeeman effect, where the internal energy levels are shifted proportionally to an applied magnetic field. As the atoms move away from the oven, the axial solenoidal magnetic field increases, keeping the transition frequency of the slowing atoms constant. By properly designing the field gradient, a single frequency can be used to slow the atoms.

The atoms are slowed sufficiently to be trapped by a magneto-optical trap (MOT). The details of how the MOT works will be described in Ch. 2. Getting both isotopes to load together was difficult because there is an optical transition in ^{6}Li that is nearly resonant with ^{7}Li, shown as the purple transition on Fig 2.2. Loading of the dual MOT has been studied in detail in past theses [1, 5, 24, 25]. It is this part of the experiment that has undergone the most modification. Any changes in power or alignment of the MOT causes the loading into the magnetic trap (MT) to decrease, which effects the radio-frequency (RF) evaporation efficiency while in the MT. Stability of the laser system, therefore, is very important.

The next step in cooling is RF evaporation in the magnetic trap. We use a clover leaf design adapted from the Ioffe-Pritchard style MT (our coil design is described in [5]). The evaporation works by spin flipping the most energetic (hottest) atoms with RF radiation. The energy level of the transition is continuously lowered and the atoms thermalize at a lower temperature. ^{6}Li cannot be evaporated in a magnetic

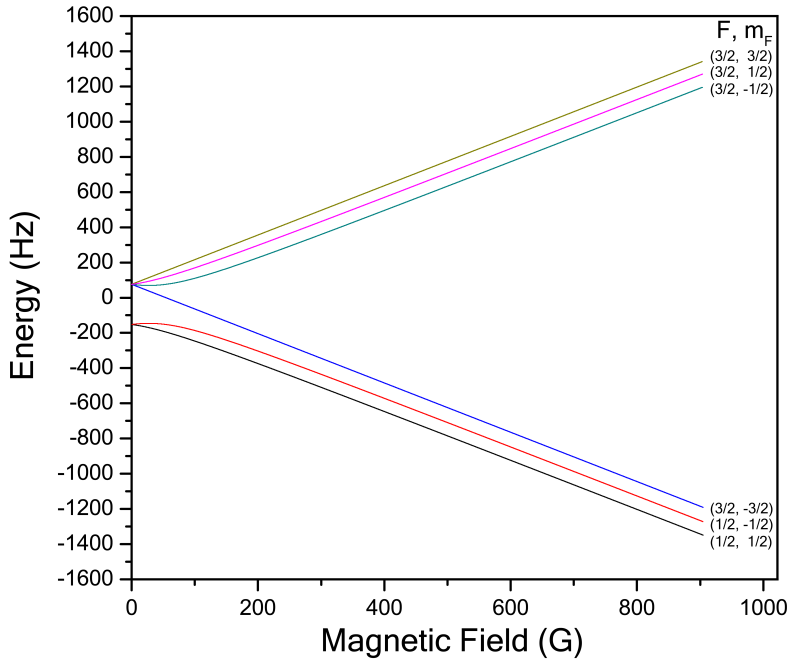

Figure 1.5 : Energy splitting of ^{6}Li versus magnetic field in the ground state. The upward sloping states are low field seeking and magnetically trappable in our trap configuration.

trap by itself, because only low field seeking states are magnetically trappable (shown in Fig. 1.5). These are states that have a positive Zeeman energy level splitting, such that $\mu \times B$ decreases with decreasing field strength. To evaporate ^{6}Li alone, we could use two states (so the fermions are not identical), but that allows spin exchange collisions. Total angular momentum is conserved, but spin is exchanged between the two atoms with $\Delta F = 1$ and $m_{total} = m_1 + m_2$. This can leave one of the atoms in a high field seeking state, causing those atoms to escape from the trap. To solve this problem, we evaporate ^{7}Li which sympathetically cools ^{6}Li during RF evaporation by elastic collisions. This dual evaporation has been optimized in the past [1, 26].

After the magnetic trap, the atoms are loaded into a single-beam trap optical dipole trap for further evaporation. The single-beam trap is made using an infra-red (IR) laser with a frequency, ω_L, detuned from the resonance frequency, ω_0. The trap works via the AC-stark shift, where the light induces a dipole moment in the atoms

which interacts as a potential [27]:

$$U = -\frac{\hbar\gamma^2}{4}\frac{I(r,z)}{I_{Sat}}\left(\frac{1}{\omega_0-\omega_L}+\frac{1}{\omega_0+\omega_L}\right). \tag{1.2}$$

The potential is defined in terms of properties of ^{6}Li, such as the saturation intensity, $I_{Sat} = 5.1\ \frac{mW}{cm^2}$, the lifetime, $\tau = 1/\gamma$ where γ=2π 5.9 MHz, and the natural linewidth, Γ=5.9 MHz. The intensity is a function of the radial distance from the center, r, and the axial distance, z:

$$I(r,z) = \frac{2P}{\pi w_0^2} Exp\left(-\frac{2r^2}{w_0^2\left(1+z/R_z\right)}\right). \tag{1.3}$$

This equation assumes a cylindrical beam with a Gaussian waist of $w_0 = 26\ \mu m$ ($\frac{1}{e^2}$ Gaussian radius). Our single beam trap has a beam which gives a typical trap depth of $\sim$200 μK at full power (2.8W at the atoms). The optical layout of our single-beam dipole trap has not changed much since Partridge's Ph.D and will not be discussed here [2].

The final step is the optical lattice which allows us to create a 2D array of 1D tubes and smoothly cross between 3D and 1D. The lattice is created by two pairs of IR beams, retro-reflected to create two orthogonal standing waves. The atoms are attracted to the intense parts of the standing waves via the dipole force. Documentation for the optics and a detailed description of the lattice can be found in Tobias Paprotta's MS thesis [28].

Chapter 2

The Magneto Optical Trap (MOT)

The MOT captures the slowest atoms moving from the Zeeman slower and accumulates them to be loaded into the magnetic trap (MT). We use both isotopes in the same trap, in what is referred to as a dual MOT and has been discussed in detail in past theses [5, 24]. This works as set of 3 pairs of counter-propagating circularly polarized beams in a spherical quadrupole magnetic field to slow and catch atoms moving at certain velocities, shown in Fig 2.1. The optical portion of a MOT works by tuning red of the trapping frequency by about 30 MHz. For ^{6}Li (^{7}Li), this is the $^2S_{\frac{1}{2}}$, F= $\frac{3}{2}$ (F= 2) $\rightarrow$ $^2P_{\frac{3}{2}}$, F= $\frac{5}{2}$ (F= 3) transition. In practice, the polarization of the MOT beams is not purely circular, and since the excited hyperfine state splitting is on the order of a natural linewidth, the probability of atoms decaying to the $^2S_{\frac{1}{2}}$, F= $\frac{1}{2}$ (F= 1) state is increased. A repump laser beam is used to pump the atoms back into the trap state, it is overlapped with the trap light and about -4γ detuned from the $^2S_{\frac{1}{2}}$, F= $\frac{1}{2}$ (F= 1) $\rightarrow$$^2P_{\frac{1}{2}}$, F= $\frac{3}{2}$ ($^2P_{\frac{3}{2}}$, F= 3) transition (see Fig. 2.2). There have recently been significant changes to everything except for the MOT coils. Therefore, I will take this opportunity to review the optical portion of the MOT and highlight the improvements that have been made.

2.1 Temperature Limits of the MOT

With the aid of magnetic fields, a MOT works by light exerting force on the atoms. Because of the red detuning, when an atom moves towards a laser beam, it is Doppler-shifted closer to resonance with this beam and can preferentially absorb a photon from it. The atom is slowed with a force proportional to the velocity of the atom [29]. The

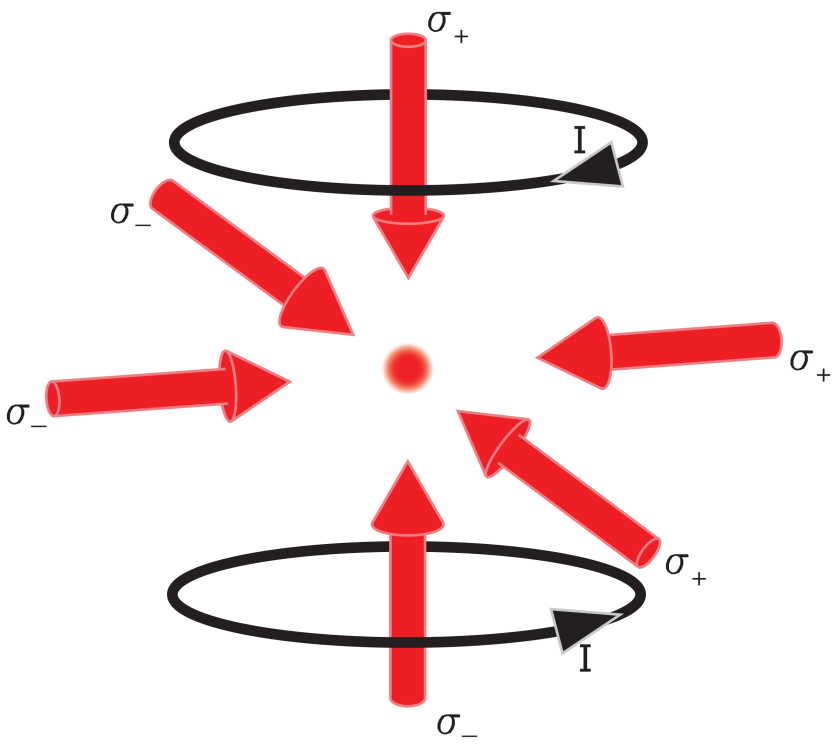

Figure 2.1 : The 3 pairs of counter-propagating beams and the anti-helmholtz coils that make the MOT. In each pair of beams, one beam is circularly polarized σ_+ the other is σ_-. Combined with the magnetic field, these beams provide the damping force and the restoring force of the trap.

magnetic field Zeeman shifts the m_j levels linearly with position within the trap. As an atom moves away from the center of the trap, the $\Delta m_j = \pm 1$ transitions becomes resonant with the $\sigma_\pm$ beams depending on the position of the atom. The force from the laser beam will push the atom back to the center of the trap. This force is proportional to the offset of the atom from center, it can thus be described as a restoring force. After many collisions, the atoms are slowed and held in the MOT.

The coldest that the atoms in a MOT can get is limited by the Doppler temperature [30]:

$$k_B T = \frac{\hbar\gamma}{4}\left(\frac{1 + 2NI/I_{Sat} + (2\Delta/\gamma)^2}{2|\Delta|/\gamma}\right). \tag{2.1}$$

This is where the force from the light slowing the atoms is balanced by the spontaneous emission. In this case, N is the number of cooling dimensions, and for this experiment

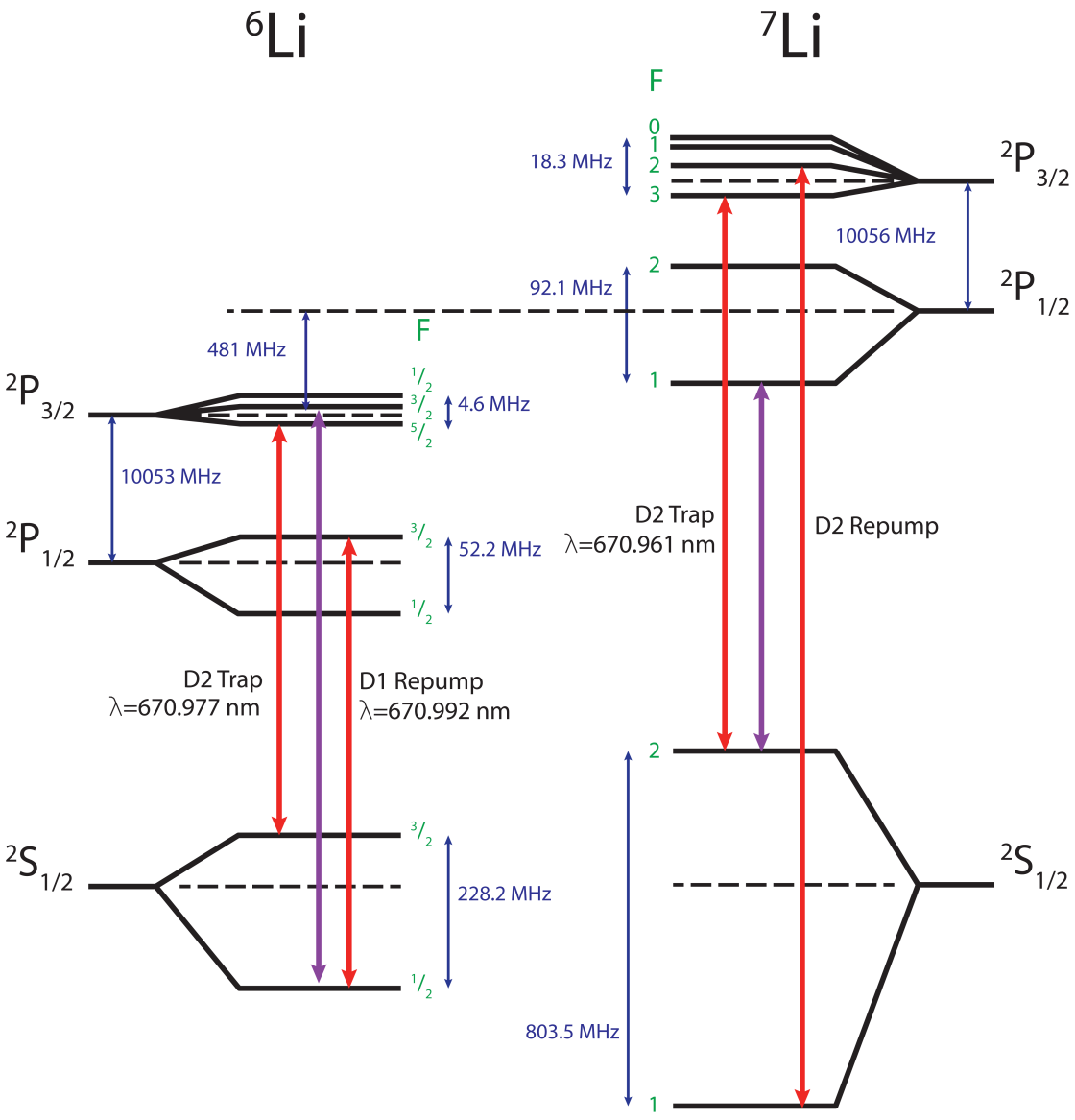

Figure 2.2 : Energy level diagram for lithium. This diagram shows the trap and repump transitions (in red) used in the MOT for each isotope. The purple lines show the transitions that are nearly resonant with one another between the two isotopes, a D2 transition in ^{6}Li and a D1 transition in ^{7}Li. It is not drawn to scale.

equals 3, and Δ is the detuning from resonance in s^{-1}. For the conditions listed in Table 2.1, Eqn. 2.1 gives a Doppler temperature of 807 μK for the ^{7}Li MOT, this is consistent with the observed temperatures that range from 800-850 μK. The minimum temperature is achieved when $\Delta = \frac{\gamma}{2}$ and $\frac{I}{I_{Sat}} = \frac{1}{3}$ which results in the Doppler cooling limit of $\frac{\hbar\gamma}{2} = 141$ μK for ^{7}Li. We have noticed on both MT experiments that the best cooling and MT loading does not occur at that limit [24, 25]. This is because the cloud becomes optically thick as it is compressed, so there is a limit to how far the light can penetrate the cloud during the compression ramp. This also limits the effectiveness of the optical pumping, since the repumping beam is unable to penetrate to the center of the cloud.

2.2 Upgrading the Laser System

Until 2011, this experiment used dye lasers as the primary source for optical power. When the entire ^{7}Li laser system was run from a single Coherhent 699 dye laser, the dye had be changed every 3-6 months which had a tendency to affect the pointing of the laser. Now we have more lasers, but no dye and still ample power. Removing these lasers resulted in large adjustments to the system, but in exchange for better long term stability. Before making these changes, we considered what frequencies and powers are necessary at each stage of the experiment.

2.2.1 The New ^{7}Li MOT

In ^{7}Li, the D2 repump transition is blue detuned 812.7 MHz from the D2 trap transition. To get the required repump frequency, sidebands were added onto the trap light using a homebuilt electro-optic modulator (EOM). This had the disadvantage that some of the laser power was lost in light that was red detuned 800 MHz, as well, since EOMs add symmetric sidebands to the carrier. Now a double passed 400 MHz

	P_{Tot}	Ratio	Δ_t	Δ_r	w_0	I/I_{Sat} per beam
^{7}Li MOT	110 mW	2	4.8 γ	3.0 γ	1 cm	2.7
^{7}Li cMOT	5.8 mW	1/7	1.7 γ	3.0γ	1 cm	0.14
^{6}Li MOT	45mW	-	3.7 γ	9.8 γ	1 cm	1.1

Table 2.1 : Typical settings for the ^{7}Li MOT, ^{7}Li cMOT, and the ^{6}Li MOT. The total power (P_{Tot}) for ^{7}Li is measured in the MOT path directly after beam splitting cube 1 with the MOT AOM at full power (labeled on Fig. 2.3). The cMOT settings are measured when the MOT AOM is set to low power at the end of the cooling and compression ramp described in Sec. 3.2 P_{tot} for ^{6}Li is measured before the beam is expanded and combined with ^{7}Li. The ratio is the trap to repump power ratio as seen on the optical spectrum analyser for the ^{7}Li light coming out of the tapered amplifier (TA), this does not apply to ^{6}Li since the TA runs at only one frequency the powers can be easily measured independently. The I/I_{Sat} is the average per beam intensity at the atoms normalized to the saturation intensity.

(IntraAction Corp., ATM-4001A1, 31% double pass efficiency) acousto-optic modulator (AOM) offsets the frequency of the light that injects a slave laser. The light from the slave laser then combines with the trap light before going into a Toptica BoosTA tapered amplifier (TA). The power available in the experiment is independent of the AOM efficiency because the TA is injected from the slave laser, additionally, no power is lost in frequencies with the opposite detuning. This allows completely independent control of the trap and repump light, which is explained further in Section 4.1. The frequencies and powers used at different stages of the experiment are given in Table 2.1.

After the TA, the light comes out of a fiber on the MOT portion of the laser table (see Fig. 2.3). Here the beam goes through the MOT AOM, which controls the total power going to the MOT. It is then expanded to have a beam waist of 1 cm and split into 6 separate MOT beams before being sent in free space over to the experiment table. Having the MOT optics separated from the rest of the table allows easy minimization of leakage light getting to the experiment table, because only the

MOT light and optical pumping light is on this part of the table.

2.2.2 ^{6}Li MOT Upgrades

In 2010, the Spectra dye laser was removed from the ^{6}Li portion of the laser system. In this configuration, light from the ^{6}Li power amplifier slave (S1) was frequency locked to the Spectra dye laser. This light traversed the entire length of the laser table to overlap on two RF photodiodes, one with light from the Spectra laser and another for the Zeeman slower master laser. The distance between the source and the lock photodiode made alignment difficult. Additionally, these were not the most robust locks. Thus, they are the focus of our efforts to improve the system. The Spectra laser produced 200 mW, which was used for the trap, optical pumping, and imaging light (see Chap. 5).

A second trap TA now stands in place for the Spectra, but it is seeded directly from the same frequency light that the Spectra was locked to, and we removed the Zeeman master altogether. The ^{6}Li Zeeman slave is injected from the TA. To offset the frequency 1.2 GHz to account for the Doppler shift of the atoms coming out of the oven, the light is double passed though a 590 MHz AOM (Center frequency 640 MHz, IntraAction, ATM 6401B2, 30% single pass efficiency) before injecting the slave.

The light coming out of the trap TA is fiber coupled and sent to the ^{6}Li side of the table. Where the trap light exits the fiber, we have added an 80 MHz trap AOM (IntraAction ATM-801A1, 90% efficiency, labeled on Fig. 4.4), this allows for independent control of the trap power. The trap light is combined with the repump light on a polarizing beam splitting cube then used for the MOT, and the light passing through the cube in the other polarization direction is used in the 2D-MOT. Then the light passes through the 40 MHz MOT switch AOM (IntraAction ADM-402AF1, 80% efficiency, on Fig. 4.4) and is expanded to match the waist of the ^{7}Li MOT light.

The light for the two MOTs is combined using a polarizing beam splitting cube (BSC 2, see Fig. 2.3). After passing through 2 beam-splitting cubes, the polarization of light for both isotopes is the same in each path.

2.3 Benchmarks

Loading enough of each isotope in the MOT is crucial for efficient loading into the MT and evaporation. To accomplish this we established a set of benchmarks in Table 2.2, below which the MOT and MT loading will suffer and the density will decrease rapidly with evaporation. It is worth mentioning that since installing the new laser system there is more than enough power and on a fresh tapered amplifier chip all the TAs are run at about 60% of maximum power. This conserves the lifetime of the chip. So, while these benchmarks must be met, they should not be exceeded by more than about 10%. At the beginning of each day, the output power from each TA and fiber should be the same as the previous day's value, otherwise the input power may have dropped and the TA or fiber may need realigning. As a last resort, the TA chip can be changed, but that is only if the benchmarks cannot be met with the TA at full power and there was a long term trend of degradation which would point to the chip. These should not be changed on a whim.

We check multiple places on each system to make sure the power is meeting the requirements; the TAs, the MOT, optical pumping and the Zeeman slower. Each of these values are measured and recorded on a daily basis in an experiment log file (found in L:\data\ emt1\"year".).

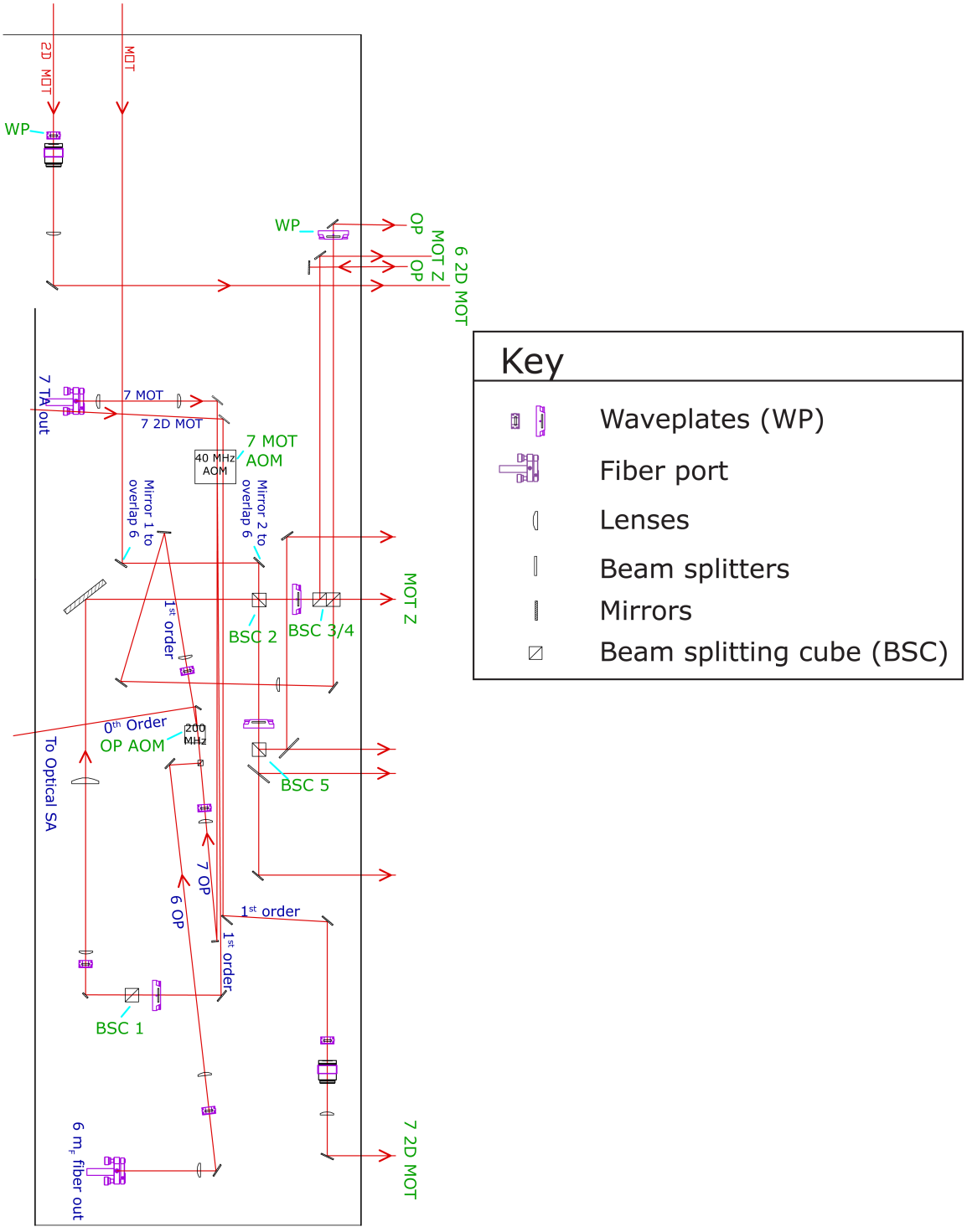

Figure 2.3 : Schematic of the MOT optics on the laser table. This shows how the light for the two MOTs are combined and how the beams are split to go over to the experiment table. This portion of the laser table also controls the optical pumping via an AOM.

Component	Minimum Power	Optimum Power
^{6}Li TA fiber	105 mW	120 mW
^{6}Li MOT fiber	55 mW	60 mW
^{6}Li trap light in MOT	25 mW	35 mW
^{6}Li repump light in MOT	13 mW	13 mW
^{6}Li Zeeman TA output	160 mW	165 mW
^{7}Li TA fiber	125 mW	140 mW
^{7}Li Zeeman TA output	220 mW	230 mW

Table 2.2 : Minimum requirements for loading the dual MOT. Less than the minimum power can result in insufficient atom number in the MOT or poor loading in the MT due to weak optical pumping. We typically run the experiment with the optimum powers, these allows for small variations with out decreasing loading. The fiber powers are measured at the output of the respective fiber. The ^{6}Li MOT powers are measured directly before the beam is expanded to a waist of 1 cm. The Zeeman TA powers are measured individually after the TA prism pair, only the freq being measured is seeding the TA, the other is blocked.

Chapter 3

The Compressed MOT

Before loading into the magnetic trap (MT), we cool and compress the MOT so the temperature of the atoms more closely match the MT trap depth. Even though the MT spatially extends around the MOT, the trap depth is on the order of 2 mK [1]. For the trap to capture the most atoms, they have to be 3-5 times colder than that.

Our average MOT starts at about 850 μK, so we need to decrease the temperature slightly. We accomplish this by cooling and compressing the MOT, a process of decreasing laser power and detunings. This reduces the temperature to around 550 μK. This leaves the temperature of the atoms at about 4 times less than the 2 mK trap depth of the MT.

3.1 Cooling the MOT

Since the MOT works via optical radiation, it is reasonable that part of the explanation for its large spatial size is determined by radiation pressure from scattered photons. If the atoms are hit with an intense beam of light on a cycling transition, then they are constantly emitting photons which causes pressure from the middle of the cloud to keep it from shrinking. When the intensity of the beams decreases, the spontaneous emission decreases as well, causing the radius to shrink. It is this process that we refer to as cooling and compressing the MOT.

3.2 Compression Ramps and Optical Pumping

We control all of the frequencies and powers for the trap and repump independently with our new control software. The software previously used for the data acquisition

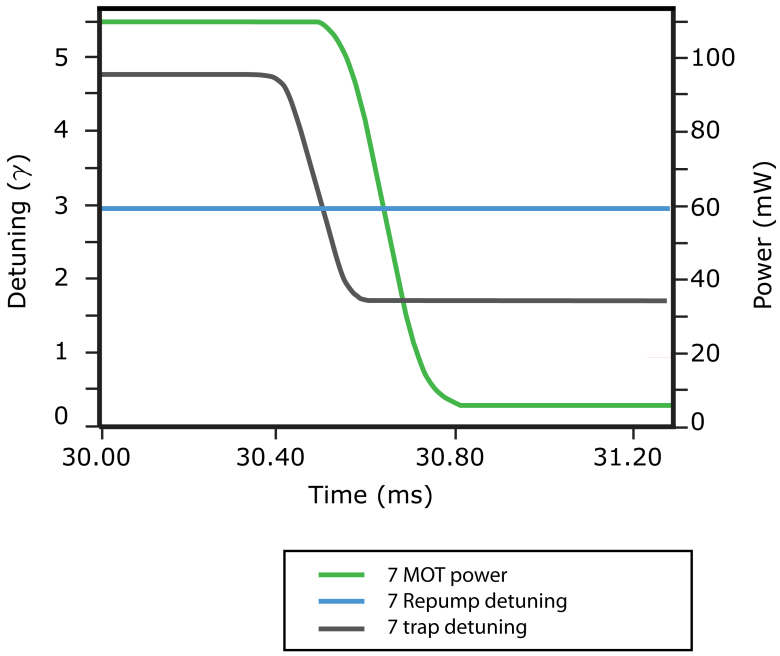

Figure 3.1 : The ramps for the ^{7}Li cMOT of the detunings and powers for the trap and repump light. All of the above voltages go to AOMs which have response times that are fast compared to the ramp time. So we may consider the ramps to be the response of the laser.

was run completely in LabView. In Oct. 2012, we replaced this software with a new program that uses sequences that have been programmed in python then run from LabView. This new software allows for changes to be made more easily to an experimental sequence. Between the new software and the new lasers we have more flexibility and finer control than in the past.

To cool and compress the MOT, we ramp the trap light from 4.8γ to 1.7γ while leaving the repump fixed at 3.0γ, after 0.12 ms the total power ramps down to 5% of the original value (Fig. 3.2). This allows all of the atoms to be pumped into the D2 trap state since they will preferentially be scattered by the repump light. The scattered light is now reduced as is the radius of the cloud, leading to a compressed MOT (cMOT), shown in a fluorescence image in Fig. 3.2.

Once the MOT coils are off we optically pump the atoms into the right hyperfine state for the MT, which for ^{6}Li is the F=$\frac{3}{2}$, $m_F = \frac{3}{2}$ state (referred to as state $|6\rangle$)

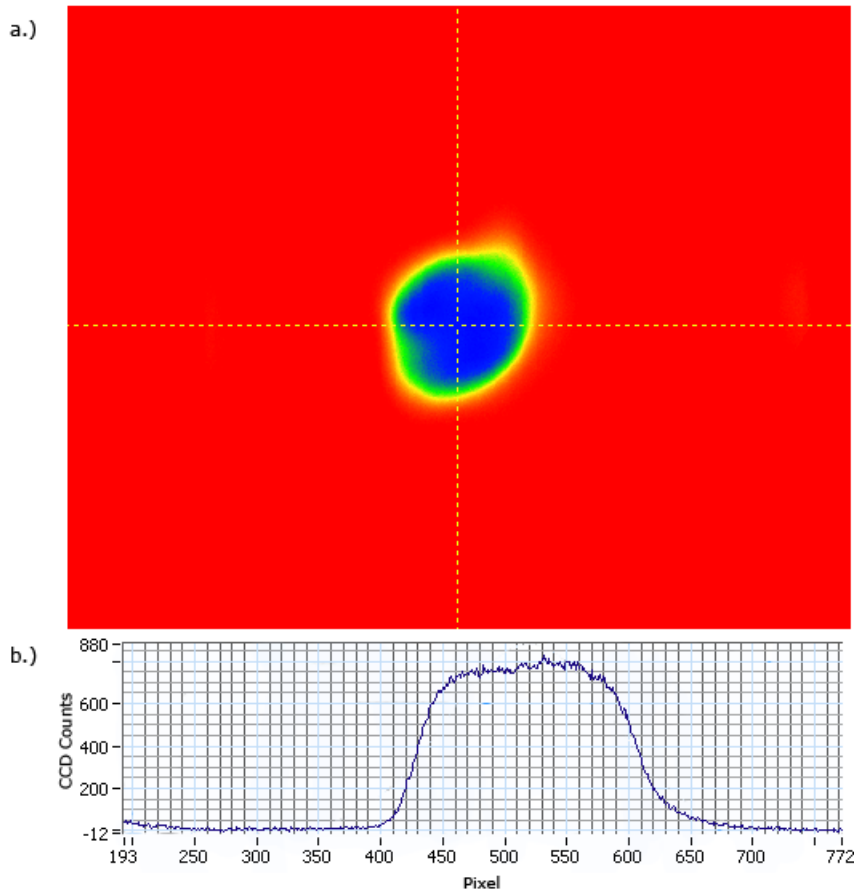

Figure 3.2 : (a.)An *in situ* fluorescence image of the cMOT and (b.) the horizontal profile, a cut through the center of the cloud along the horizontal axis. The image was taken with a 0.1 ms exposure and 0γ detuning. The cMOT appears flat topped because the optical density is too high for the MOT beams to penetrate to the center of the cloud.

and for ^{7}Li is the F=2, m_F=2 state (the $|2,2\rangle$ state). With the new laser system, the available power for ^{7}Li optical pumping has been cut from 240 mW to 100 mW. As a result, we have lengthened the optical pumping times by about 0.2 ms and decreased the detunings by 40 MHz. This is the one place in the laser system where the power was not conserved, but we could afford the loss, after adjusting the optical pumping parameters, will still obtain the same loading efficiency into the MT (20%). The best optical pumping is achieved when the optical density is low, therefore the detuning must be large, 33γ for ^{7}Li. But, there still must be 10 photons scattered

	P_{mF} high	P_F high	P_{mF} low	P_F low	Δ_{mF}	Δ_F	δt
^{6}Li	12.0 mW	13.0 mW	12.0 mW	2.0 mW	66 MHz	58 MHz	0.6 ms
^{7}Li	83 mW	16 mW	66.0 mW	33.0 mW	196 MHz	175 MHz	0.7 ms

Table 3.1 : The optical pumping parameters for optimal loading into the MT. We have a the optical pumping split into two parts. The first half the F-pump power (P_F) is at the same power it was in the MOT. In the second half, the mF-pump power (P_{mF}) dominates. We have found without either of these the optical pumping is incomplete, most likely due to the optical thickness of the cloud.

per atom, this ensures that atoms in any hyperfine state of the F=2 level can reach the $|2,2\rangle$ state via Δm=1 transitions. The number of photons scattered is related to the fraction of atoms the excited state, ρ_{ee}, and the duration of the probe, δt, by [29]:

$$N_{Scatt} = \frac{\gamma \frac{I}{I_{Sat}}}{4\frac{\Delta^2}{\gamma^2} + 2\frac{I}{I_{Sat}} + 1}\,\delta t \;=\; \gamma\,\rho_{ee}\,\delta t. \tag{3.1}$$

The duration of the optical pumping is 0.7 ms for ^{7}Li and 0.6 ms for ^{6}Li. Halfway though we change the ratio of the m_F to F pump light, the powers during each portion are given in Table 3.1. Using the parameters from Table 3.1 and Eqn. 3.1, we get an average of 15.0 photons scattered per beam for the ^{7}Li m_F pump and 21.3 photons scattered per beam for the ^{6}Li m_F pump. To experimentally insure we have significant optical pumping power, we compare the number in the MT for different optical pumping times, see Fig. 3.3. If the number starts to plateau, there is sufficient optical pumping, however, if the number is still climbing, then the detuning, power, and beam waist should be adjusted to optimize the efficiency. It is clear in Fig. 3.3 that the optical pumping is saturating around 0.35 ms for the F pump detuning of 23γ.

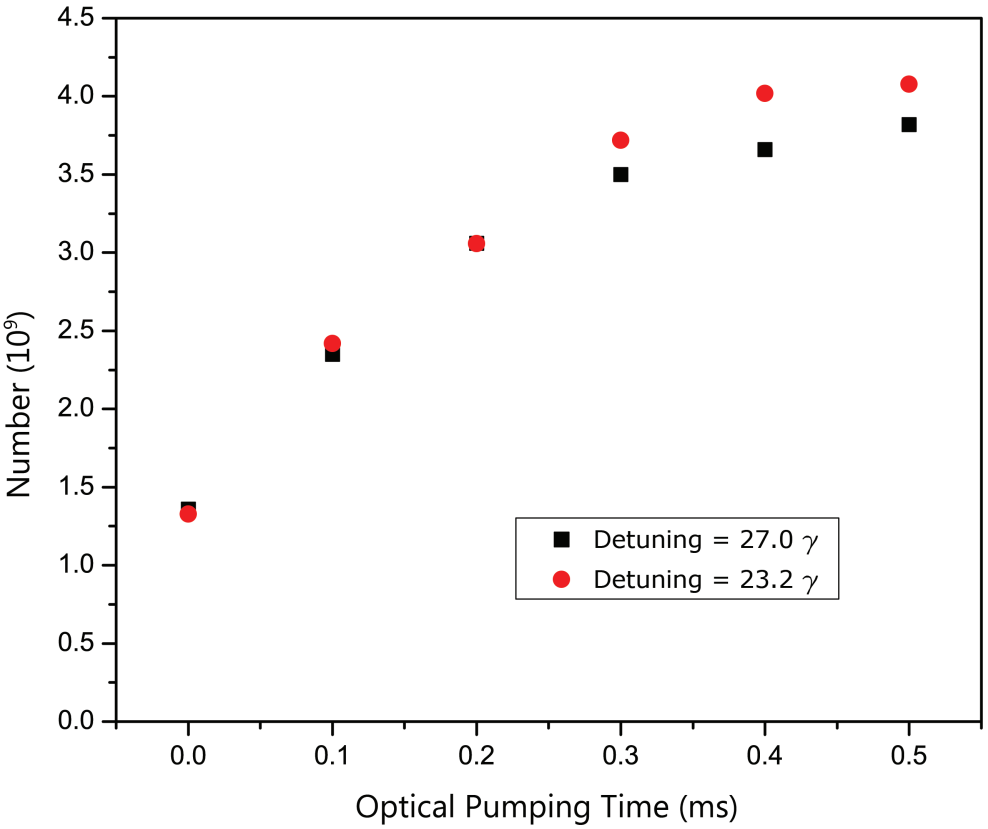

Figure 3.3 : Number of atoms in the MT versus optical pumping time. When the number saturates the optical pumping time is sufficient. This shows the number when the optical pumping settings are adjusted for the first half of the optical pumping and the F pump detuning is varied.

Chapter 4

The New Laser System

As discussed in Chap. 2, there were many aspects to consider when changing the laser system, one of the most crucial was the conservation of the total power. The new laser system only has 2 TA's for the majority of the power for the MOT's and 2D-MOT's and 1 TA for the Zeeman slowers, where we used to have 2 dye lasers. For the new system to provide the long term stability that we need, it is important that no single component runs at 100% for the system to function, this includes the output power of the TA's. We also want enough power coming out of the TA's so that they can be initially turned down to less than maximum power to extend their lifetime. Another important aspect was improving the locks of the master lasers such that they would be reliable over the course of the day.

4.1 The ^{7}Li Laser System

The heart of the new laser system begins with the new master laser (an extended cavity diode laser). This laser is locked to the heat pipe and controls the frequency stability of all the lasers that are locked to it. To replace the Coherent dye laser we installed a Toptica DLPro. It has a center wavelength of 670.8 nm, a typical power output of 16 mW and a mode-hop-free tuning range of approximately 10 GHz. It easily scans over the entire ^{7}Li spectral feature as seen in Fig. 4.1.

The DL Pro injects a power amplifying slave laser (S5), all of the slave lasers are homebuilt and use a Hitachi HL6555G diode, except for the ^{6}Li power amplifier slave and ^{6}Li Zeeman slave. This gives us 50 mW after the S5 laser isolator to inject the three slave lasers for the ^{7}Li system that control the trap, repump and Zeeman light

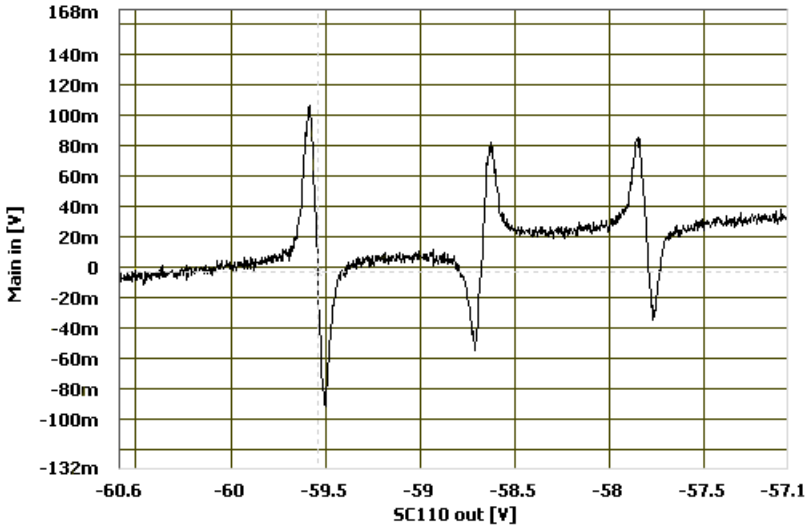

Figure 4.1 : The ^{7}Li saturated absorption features versus the piezo scan voltage on the DL Pro. We lock the laser to the left most feature, the $^2S_{\frac{1}{2}}$ F= 2 $\rightarrow ^2P_{\frac{3}{2}}$ F= 3 transition. On the right is the $^2S_{\frac{1}{2}}$ F= 1 $\rightarrow ^2P_{\frac{3}{2}}$ F= 2 transition and in the center is the crossover feature between these two transitions.

(Figure 4.2). The trap and repump lasers are each injected after a double passed AOM, the repump offset 400 MHz AOM (mentioned in Sec. 2.2.1) and the trap offset AOM which has a center frequency of 80 MHz (IntraAction ATD-801A1, 60% double-pass efficiency). These AOMs have a scanning range of approximately 20 MHz for a single pass without unlocking the laser they inject. The frequency as a function of control voltage on the voltage controlled oscillator (VCO, from Mini-Circuits, part numbers: ZOS-535+ and ZOS-100+ respectively) for each offset AOM is given in Fig. 4.3. The Zeeman slower frequency is set by a 1.2 GHz AOM (homebuilt, $\sim$10% efficiency) that injects the last slave on the new laser system. Each of these slave lasers receives 1-4 mW of light at the injection port of the isolator.

4.2 Updates to the ^{6}Li Lasers

After removing the Spectra dye laser from the table, not many changes needed to be made. The TA seed slave (S3) was added and the power amplifier slave (S1, Phillips

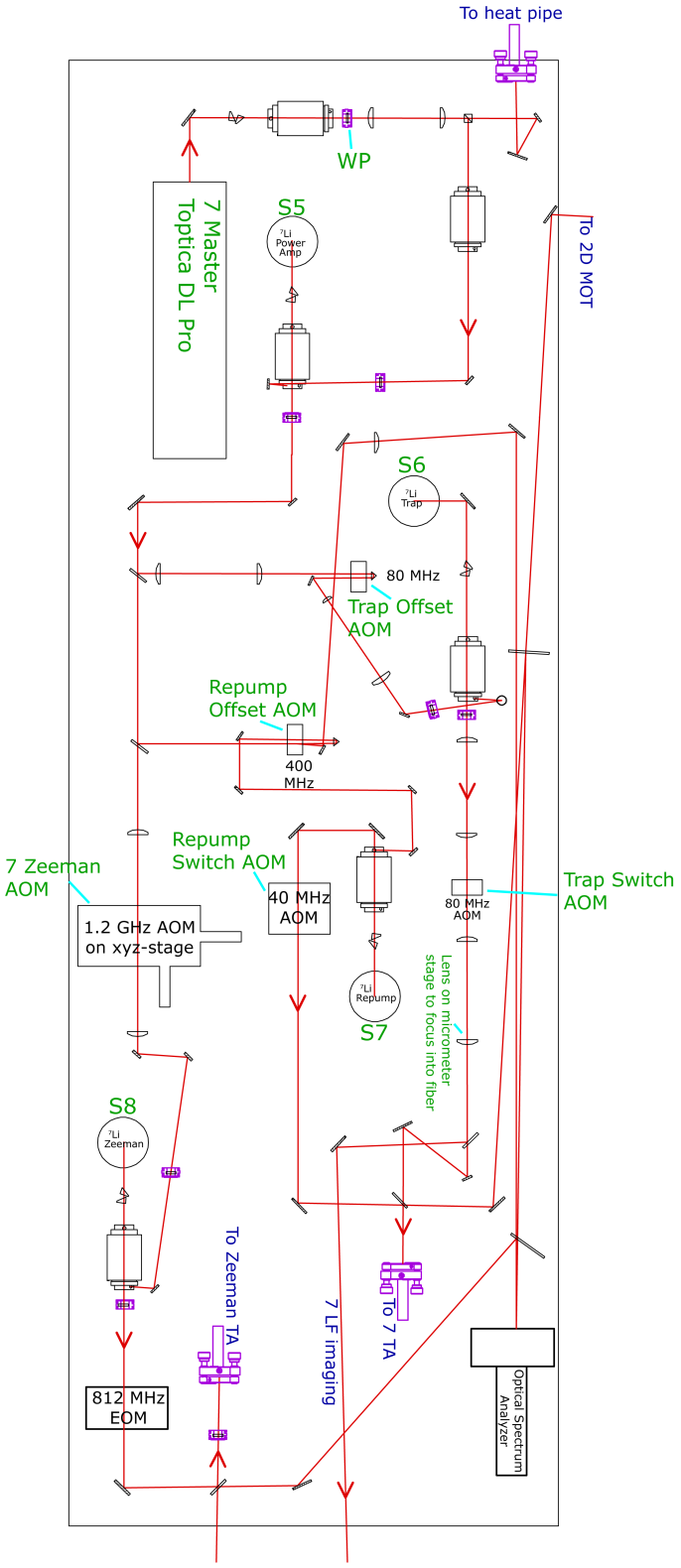

Figure 4.2 : Layout of the ^{7}Li portion of the laser table. The two double passed offset AOMs for controlling the detuning of the trap and repump light are near the center of the drawing. The trap and repump light combines at a beam splitter and injects a fiber where it goes to the ^{7}Li TA.

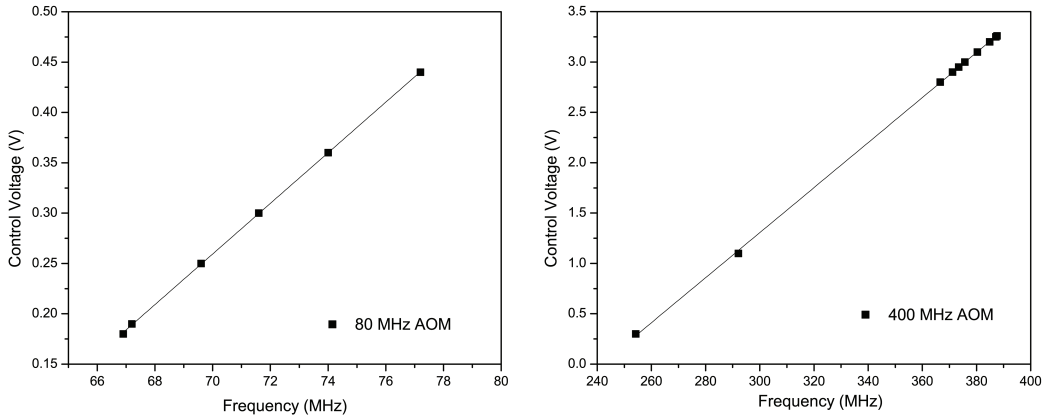

Figure 4.3 : The frequency of the trap (left) and repump (right) double passed AOMs as a function of control voltage on the VCO.

diode, ∼10 mw output power) path was modified to increase stability, see Figure 4.4, but the master laser's optical path and the heat pipe path has stayed mostly unchanged since Partridge's MS thesis [24]. The most significant change is to the heat pipe lock and current controller of the heat pipe master laser (M1). This laser locks to the crossover and all of the lasers are locked to it.

Originally, this laser had a scan range of ∼0.7 GHz and would come unlocked from the heat pipe multiple times a day. We found the primary reason for this was the lack of feed forward in the current controller. There was no independent gain for the piezo or the current in the original current controller. We replaced this controller by a design implemented by Apparatus 3 [31] that immediately improved the lock time and the scanning range to greater than 7 GHz. The laser now easily scans over the entire ^{6}Li saturated absorption feature as seen in Fig. 4.5. Now all the master lasers on the experiment run off a similar design.

The heat pipe master injects a power amplifier slave (S1) which injects the TA seed slave (S3). The dual slave system is necessary due to the limited power and poor mode matching in the injection path coming from M1. There is only ∼1 mW for the injection lock where we have seen we need about 2 mW with poor spatial modes to inject a high power diode (Hitachi HL6555G), which is required to seed the TA

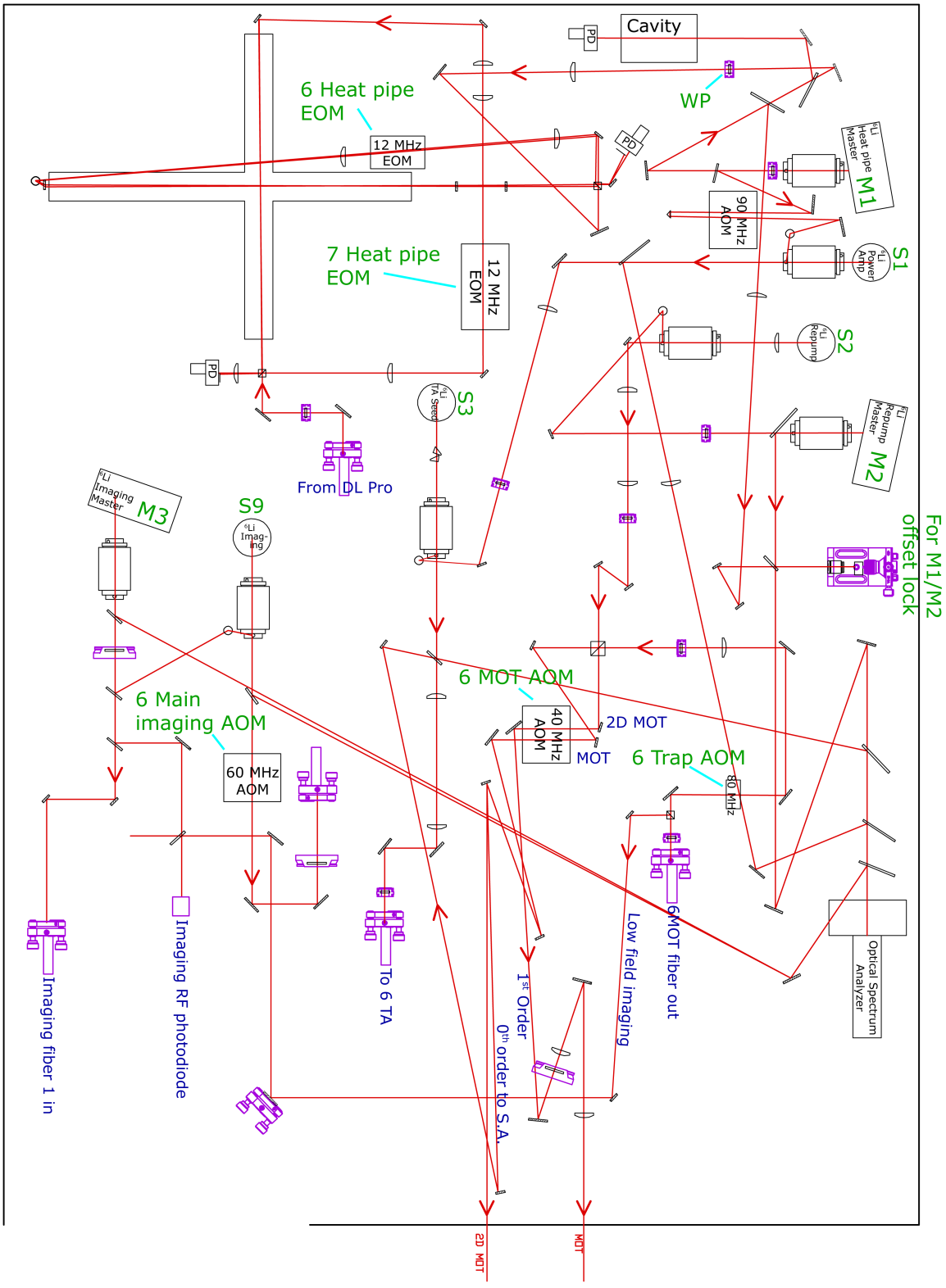

Figure 4.4 : Diagram of the ^{6}Li section of the laser table. The large cross at the top is the heatpipe where ^{6}Li is in the horizontal direction and ^{7}Li goes through in the vertical direction (on the layout).

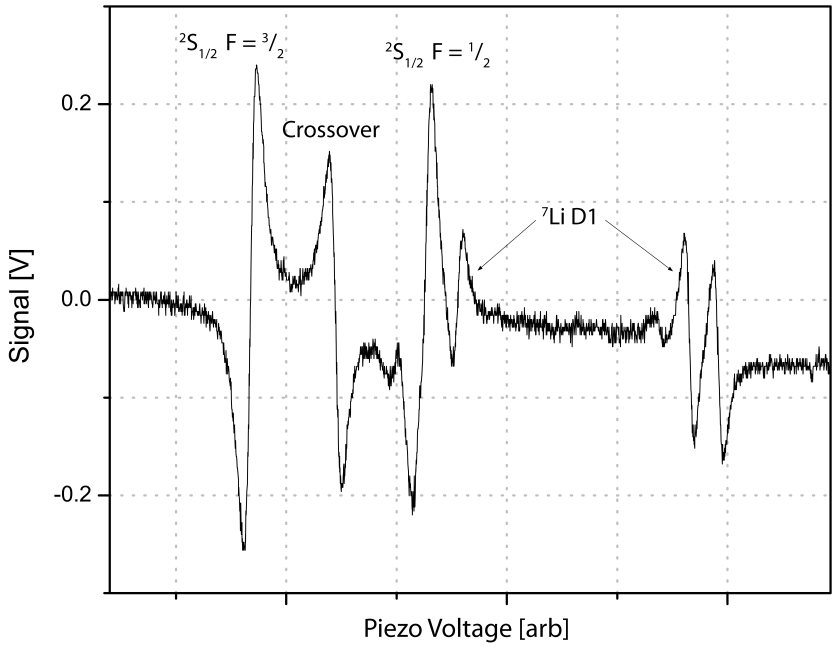

Figure 4.5 : The ^{6}Li saturated absorption feature as seen on the oscilloscope when locking the laser. The laser scanning range can be as large as 7 GHz if the feedback is adjusted well. Shown here is a scanning range of 1 GHz, the ^{6}Li features are on the left, the feature on the right is due to crosstalk with the D1 lines of ^{7}Li in the heat pipe (as is the distortion of the saturated absorption signal.)

(>25 mW). The power amplifier slave is run from a low power diode, it only produces around 9 mW after the isolator, but that is more than sufficient to inject S3. With better mode matching, the power amplifier slave would not be necessary. However, the proximity of S1 to M1 does give us the opportunity to ramp the frequency if we desired (we do not currently use this feature, but it is simple to implement in the future if desire with the current optics layout and control software).

For ^{6}Li, the repump frequency is 10 GHz from the crossover, therefore we use a second master laser that is frequency offset locked to M1. The repump master laser (M2) then injects a repump slave laser (S2) that combines directly with the trap light to become part of the MOT.

4.3 Overview

Now that each part of the laser system has been address independently (except for imaging), I will show how it all fits together in Fig. 4.6. There are a few places where the different systems overlap, such as the Zeeman slowers. The imaging light comes from a fiber at the opposite end of the table because of the frequency reference (this will be discussed in Section 5). Also, the ^{6}Li MOT and 2D MOT light passes free space from the 6 laser section to the MOT portion of the table. Overall, the table is sectioned off with select laser beams crossing the dividers, and each table section fits together as shown in Fig. 4.6.

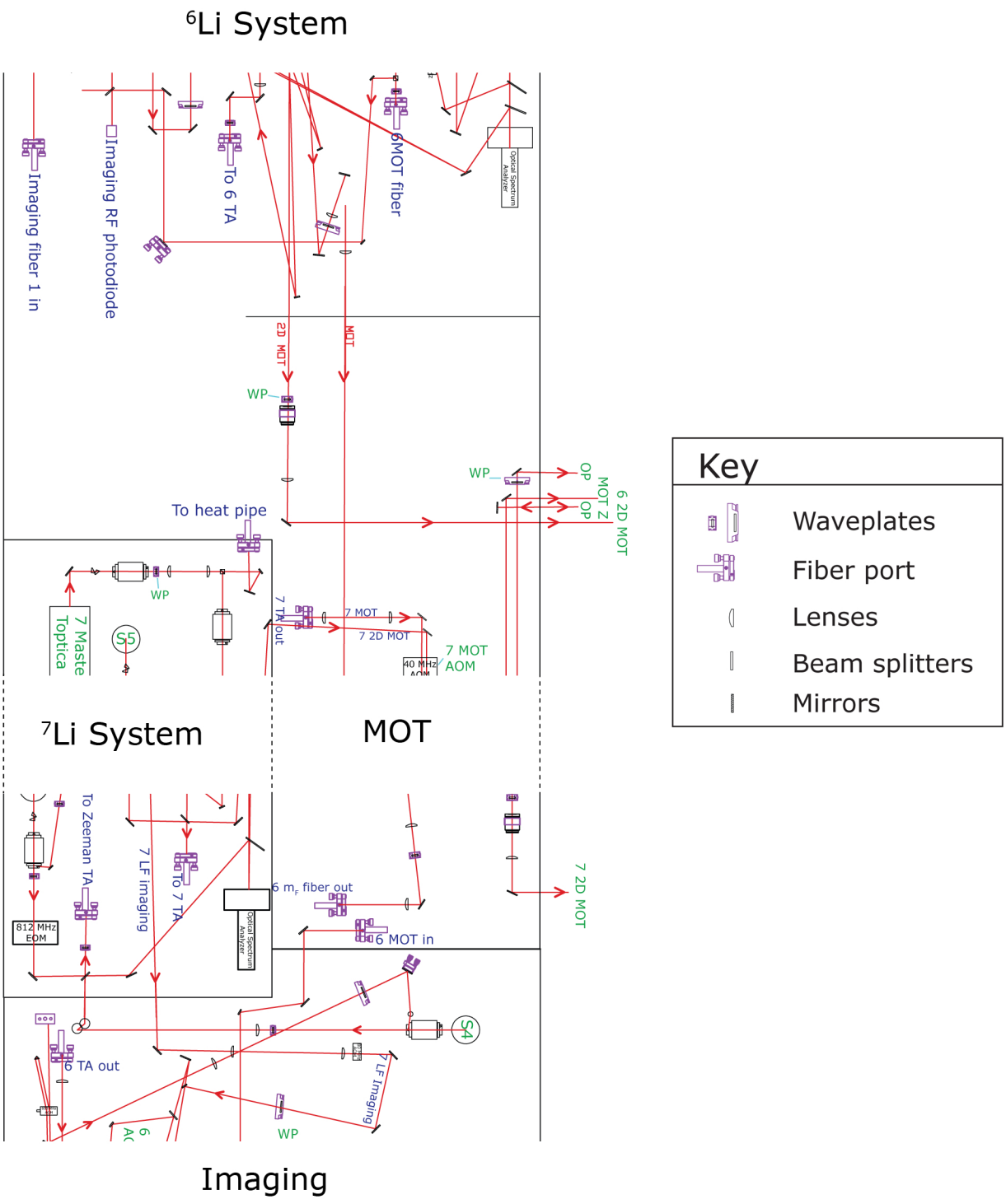

Figure 4.6 : Since the schematic is so large, it has been also divided into sections to make it easier to see the detail. This shows how each of the previous sections (labeled) fits together and where laser light crossed a boundary from one section to another. The cadd drawing for the full schematic can be found in "L:\docs\cadd\emt1\lasertable_v8.dwg".

Chapter 5

Imaging

After replacing the Spectra laser and changing from the Andor camera to the Coolsnap camera [3], we realized we lost a few essential tools. The Spectra laser has a large tuning range and was frequency offset locked to M1, allowing its frequency to be adjusted by GHz during MT evaporation. This made it possible for us to image any ^{6}Li $^2S_{\frac{1}{2}}$ hyperfine state at any magnetic field. When we removed that laser, only the imaging AOMs could provide the frequency offset for the imaging. These have a relatively fixed frequency, and we could only image the lowest two hyperfine states of ^{6}Li near the Feshbach resonance which we use for evaporation in the dipole trap. We added trap light in a separate path to image state $|6\rangle$ at zero field, but there was still no light to image state $|6\rangle$ at fields near the Feshbach resonance.

Additionally, the Andor camera had a slightly larger field of view than the Coolsnap camera. This allowed us to take time of flight images of the cMOT and MT to get temperatures in the past. When we switched cameras, while we gained the ability to take fast images, we lost fluorescence time of flight imaging except when the cloud was mostly evaporated. Fortunately, we have found solutions to these problems.

5.1 Basler Camera

To get accurate temperatures of our cloud in the early stages of the experiment, we must be able to take time of flight (TOF) images. The field of view of our main imaging camera is insufficient for this in the MOT and unevaporated MT. To solve this problem, we have installed a second camera (the Basler Scout scA1000) perpendicular to the Coolsnap camera. This camera has a second advantage, it allows a second point

of view when loading a MOT to look for abnormalities in the shape of the cloud. The Basler has a fixed focus lens (Navitar TV Zoom 7000), so we can zoom the camera in and out, but the focal point will remain the same. For daily use we have found a 30 μm/pixel zoom to be most useful.

5.1.1 Fluorescence Imaging

We use the MOT beams for imaging to get uniform fluorescence. Typical imaging parameters are 0γ detuning for a duration of 100 μs or less. A longer pulse will cause the cloud to deform from the force of the light. For clouds that have a higher phase space density such as the *in situ* cMOT and especially the evaporated MT, detuning the lasers might be necessary. For fluorescence imaging of ^{6}Li, we typically use a longer pulse because the detuning is fixed at 5γ from resonance. We leave the detuning fixed at the MOT frequency because we have not incorporated frequency control for the ^{6}Li trap light. Figure 5.1 shows an example of a fluorescence image for ^{7}Li and ^{6}Li.

5.1.2 Imaging Analysis

Similar to absorption or phase contrast imaging, the first part of analyzing a fluorescence image is normalizing the signal [3]. We take two images with each run, one with atoms and one without for normalization. A reference image is also used to subtract readout noise, bad pixels and stray light from both the atoms and the no-atoms image. To get a number from a fluorescence image, we must count all the photons on the CCD. It is important to remove the excess light and not clip any of the cloud. We supply a bounding box, for which all the counts inside are added (C_A, the atoms image) and all the stray light (C_{NA}, the counts on the no-atoms image) is subtracted, so the no-atoms subsection is subtracted from the atoms subsection.

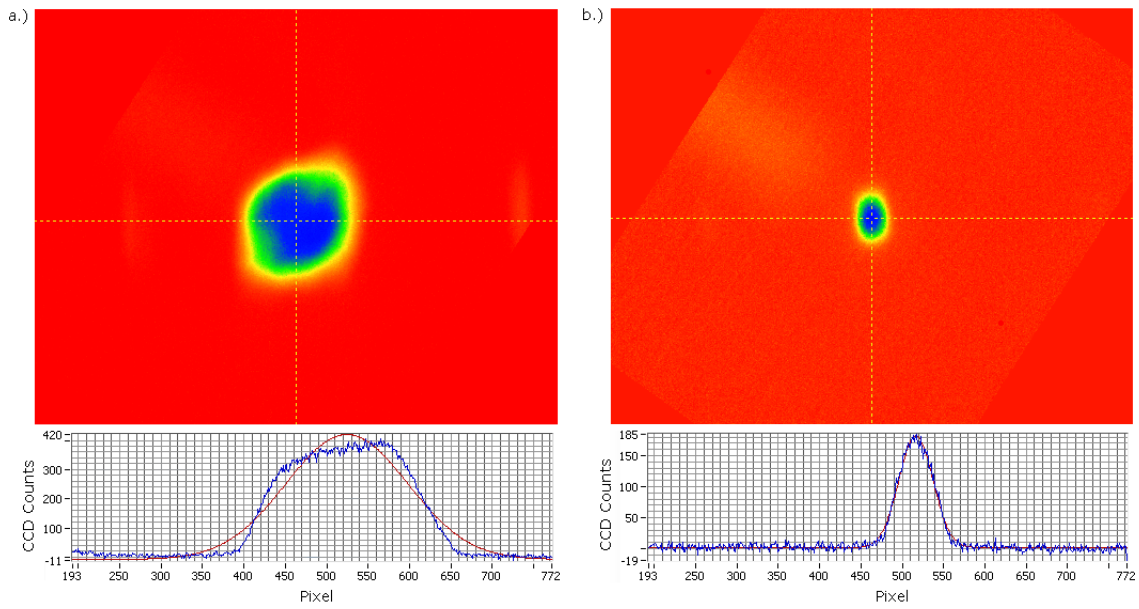

Figure 5.1 : A fluorescence image of (a.) the ^{7}Li MOT and (b.) the ^{6}Li MOT. These images were taken from a point of view 90° different from that of the Coolsnap camera. The ^{7}Li MOT image was taken under typical experimental settings of 0.1 ms, 0γ detuning, and 0 ms time of flight. The lithium ^{6}Li exposure setting were the same except the detuning was set to 5γ. The profiles underneath are (blue) the horizontal cut through the center of the cloud and (red) a Gaussian fit to the cut.

This leads to an equation for the total number of atoms:

$$N = \frac{(C_A - C_{NA})}{Q\rho_{ee}\gamma t g}, \tag{5.1}$$

which depends on the pulse length of the imaging beams (t). We also account for the small fraction of the photons that were collected by the camera since fluorescence is omnidirectional (g is the solid angle of the camera collection area). We determined the solid angle to the camera by adding an iris in front of the lens and closing it until the signal begins to decrease. We convert the counts to photons via the camera efficiency (Q) and we get the total number of atoms in the cloud. The quantum efficiency is 47%, given in the Basler manual [32].

After getting a number, we fit the cloud to a Gaussian to get a radius. This allows us to determine a temperature using:

$$r^2 = r_0^2 + 2\frac{k_B}{m_L}T(t - t_0)^2, \tag{5.2}$$

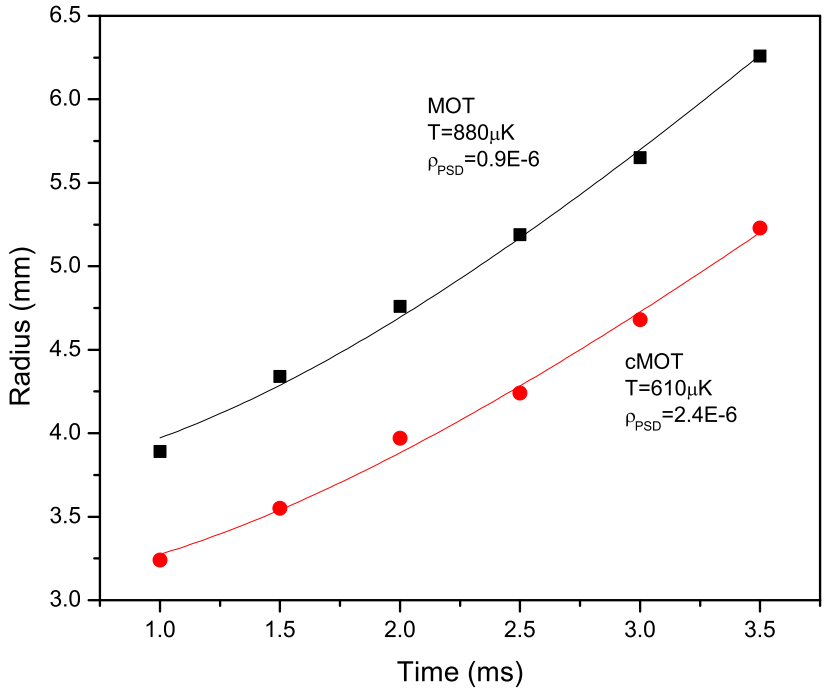

Figure 5.2 : A time of flight series for the ^{7}Li MOT and cMOT. We let the cloud expand for 1 ms before trying to fit to a Gaussian because it is too dense to get an accurate fit at short time of flights. We typically only use the temperatures obtained from fitting the vertical waist to insure there was no interference from the cloud approaching the window of the chamber.

where r_0 is the Gaussian $\frac{1}{e}$ radius and m_L is the mass of the relevant isotope of lithium [33]. We release the clouds in intervals of 0.5 ms from 1-3.5 ms (see Fig. 5.2), at 3.5 ms the cloud begins to get too close to the windows inside the chamber.

5.2 Using the Basler to Align the Single-Beam Trap

After changing a MT coil or removing one from the chamber, the single-beam trap is no longer aligned to the MT. The position of the MT is very sensitive to the placement and wrapping of the coils, as any small change can move the MT radially by hundreds of microns. With the single-beam trap having a waist of only 26 μm, and the MT having a radius of 50-100 μm, it is easy for the traps to not overlap with each other.

Before the installation of the Basler, finding the single-beam trap used to involve some tricky geometry, a bit of guessing, and a very long 2D search. The Basler camera is perpendicular to the single-beam and has within its field of view both windows that the single-beam passes through. Since the MT is roughly centered on the Basler field of view, we have narrowed this down to a 1D search.

Evaporate the MT down to 1-2 MHz above the trap bottom and take a fluorescence image on the Basler. Mark the position of the MT and adjust the focus to look at the laser table side window where the fluorescence from the single-beam is seen. Turn the single-beam on and move it such that it aligns vertically with the position of the evaporated MT (see Fig. 5.3). Using this method, we have found the dipole trap position in the vertical direction on the Basler is usually correct within 90 μm (3 pixels on the Basler). If the 1D search is conducted using a cloud evaporated to 15 MHz above the trap bottom, a 2D search should not be necessary.

5.3 The New Imaging Laser

In the old laser system, part of the Spectra laser power was picked off and used for imaging. Without the tunability of the Spectra we lost the ability to image ^{6}Li in state $|6\rangle$ at non-zero fields and states $|1\rangle$ and $|2\rangle$ at fields less than about 700 G. In order to diagnose the efficiency of transferring atoms from state $|6\rangle \rightarrow |1\rangle$ in the single-beam trap it is necessary to image both states at the same field.

For this we installed a new imaging master laser which is side-of-filter frequency offset locked to the output of the ^{6}Li TA and injects an imaging slave laser for additional power. The side of filter technique uses the beat note between two master lasers on an RF photodiode to feedback to the second laser (the imaging master) [34]. The output of the photodiode is mixed with a synthesized RF source, in our case the frequency comes from one of three VCOs (Mini-circuits) depending on the frequency

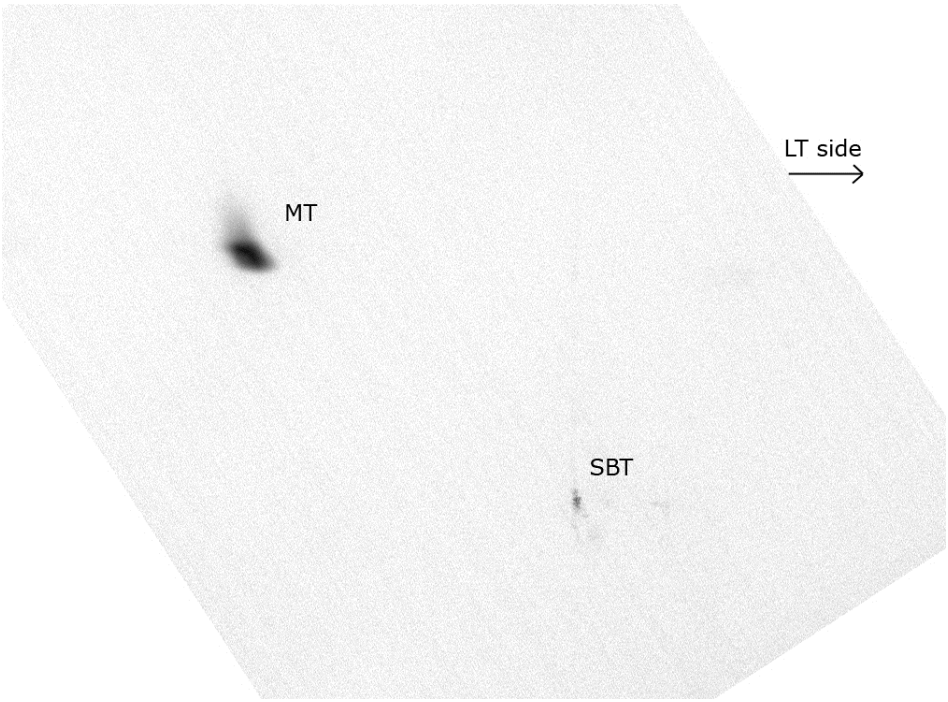

Figure 5.3 : A fluorescence image with the MT and the single-beam trap. It is clear they are misaligned vertically with respect to one another. The image has been rotated such that the single-beam axis is aligned to the horizontal axis. The visible spot from the single-beam trap (SBT) is from passing through the laser table (LT) side chamber window.

range we intend to lock to. The mixer output goes to a splitter, which we connect to a frequency counter to monitor the frequency of the lock. This is followed by another splitter, one output is attenuated by 6dB, the other output has a high-pass filter with a 3dB point of 164 MHz and a 3dB attenuator, this defines the lock point of the circuit. After the attenuators, each path is converted into a DC voltage and added together, which is used in a servo and fed back to the second master laser to control the frequency.

The imaging laser has a maximum frequency offset locking range of ±30 MHz to ±1.265 GHz. The light then passes through the main imaging AOM (currently set to +70 MHz, IntraAction ADM-70, 78% efficiency) which controls light input to imaging fiber 1 (see Fig. 5.4 and 4.4). After the fiber there are two imaging AOMs, the first order of these control the light aligned to imaging fiber 2. The single pass imaging

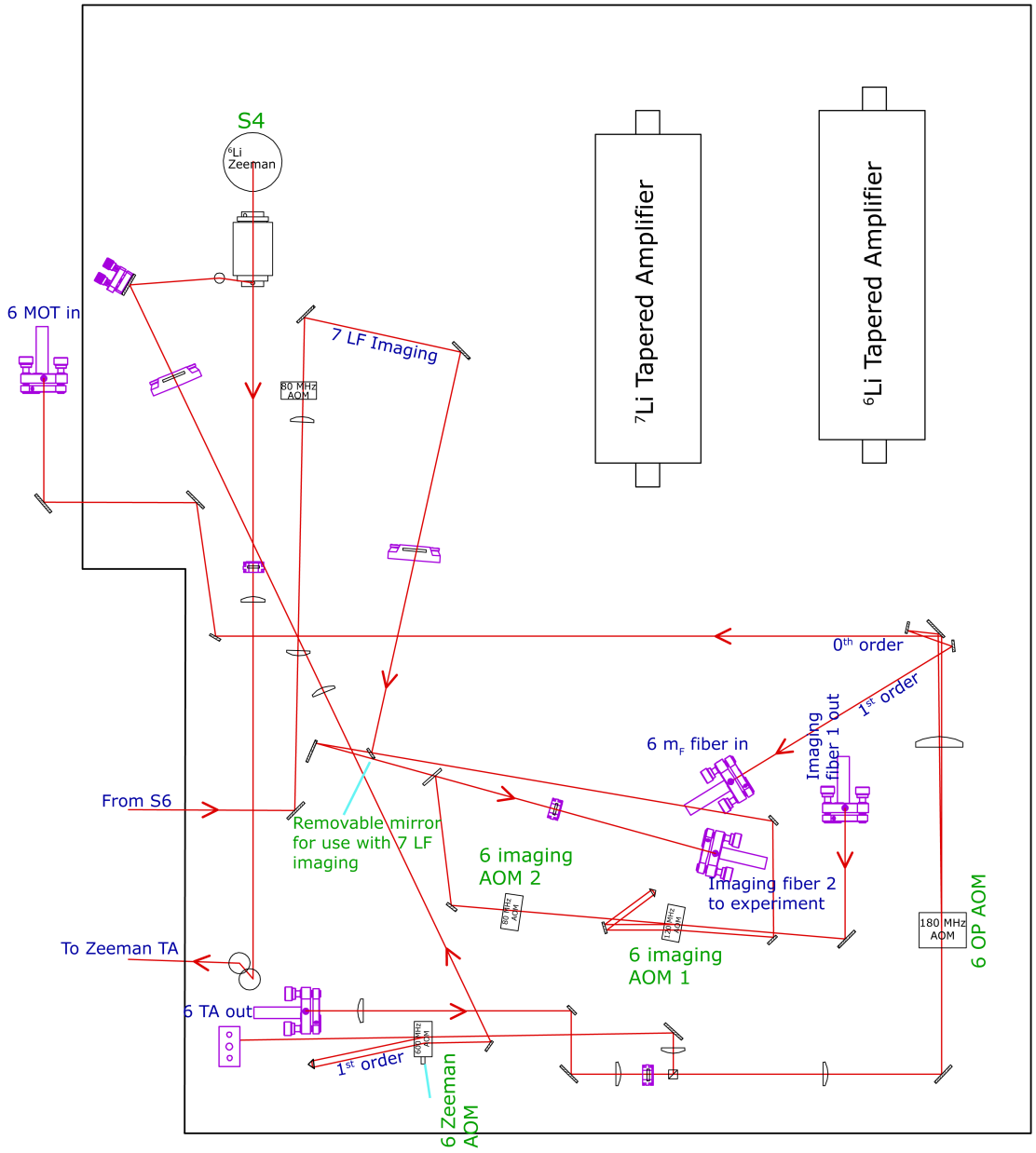

Figure 5.4 : Layout of the imaging portion of the table. The old imaging system begins from the output of imaging fiber 1. The fiber passes the light from the new imaging slave to this end of the table. It has the advantage of keeping the two parts of the imaging system isolated, if any changes need to be made only half needs to be realigned.

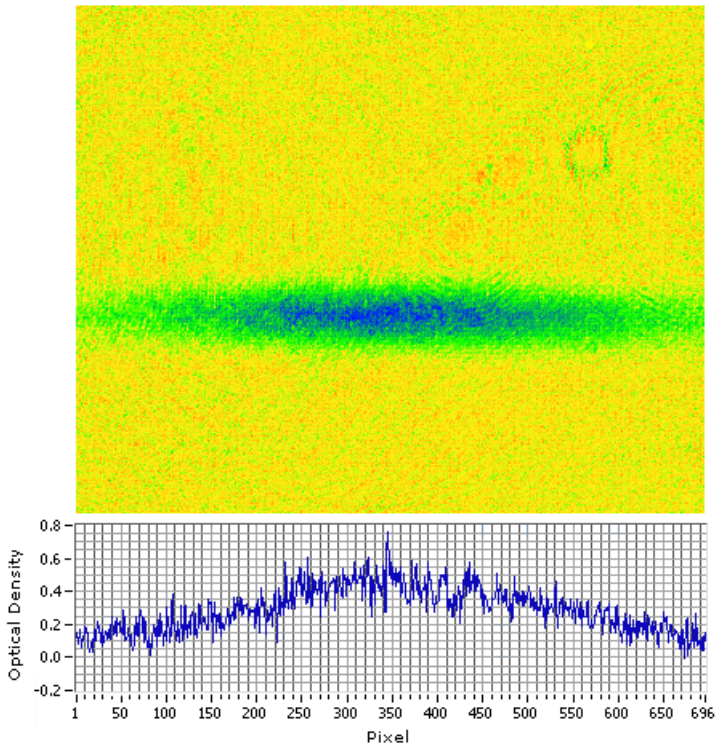

Figure 5.5 : Using the new imaging laser we have the ability to easily take images that are detuned from resonance and image all the states of interest for ^{6}Li. Shown here is an on resonance absorption image of state $|6\rangle$ at 830 G using the single imaging mode with 0.3 ms time of flight (this allows us to use the entire CCD). The imaging master is locked to +1260 MHz for this image.

AOM 2 (80 MHz center frequency, 77% efficiency, Crytral Tech. 3080-151) is less red detuned than the double passed imaging AOM 1 (120 MHz center frequency, 18% double-pass efficiency, IntraAction ATD-1001A1). For dual on resonance absorption, imaging AOM 2's frequency is tuned to state $|1\rangle$ and imaging AOM 1 is set for state $|2\rangle$. Between the large tuning range and the AOMs, we can image states $|1\rangle$, $|2\rangle$ and $|6\rangle$ for fields from 0-910 G (see Fig. 5.5).

5.4 Benchmarks

It is important to know some of the common settings for the imaging master to image different states. We lock to a frequency different than the imaging transition by the offset of a couple AOMs. Table 5.1 shows some of the standard frequencies we use for

State	$\|6\rangle \rightarrow \|e\rangle$, B=0 G	$\|6\rangle \rightarrow \|e\rangle$, B=836 G	$\|1\rangle \rightarrow \|e\rangle$, B=836 G
Frequency	95.5 MHz	1260.0 MHz	-917.5 MHz

Table 5.1 : Some common imaging frequencies for the imaging master laser to when running the experiment. Until we get into the single-beam trap, state $|6\rangle$ at B=0 G is used. The sign determines whether the lock should be set in red or blue mode as the laser can be tuned either way (red = negative and the direction is labelled on the scope used for locking.)

running the experiment. We use on resonance imaging at zero field to calibrate the offset and extrapolate from there for any field. The frequency offset of the master is defined through imaging AOM 2 for the 1st image, since it can be used when the ^{7}Li zero field imaging is in use (which blocks the imaging AOM 1 optical path).

When the imaging system is well aligned, there should be >25 mW out of imaging fiber 1 in steady state mode. Each imaging AOM after fiber 1 should have around 4 mW entering imaging fiber 2 in steady state mode. These powers should not drop when pulsing the AOMs, but they cannot be easily measured with the power meter in pulsed mode. Measure the steady state powers on a photodiode and ensure the voltage on the photodiode in pulsed mode is the same. At least one of the AOMs will need to be re-aligned when pulsed (we have a video sub vi for this procedure).

Chapter 6

Conclusion

I'll will give some tips for trouble shooting various new devices and reiterate some helpful hints from the past. Though these improvements are extensive, they are not the last, so I will point out where to expect some future modifications. The point of improving the experiment was to make it more robust and reliable so we can continue studying physics but with less interruptions for repairs and realignments. I will also address what direction our research is headed, now that the modifications are finished.

6.1 Troubleshooting

The heat pipe master lasers are rarely aligned into a wavemeter fiber, but the correct mode can be found by looking into the heat pipe. Note - this is useful for mode jumps but not for a new diode. Since our heat pipe is cross shaped, we can look in one side without blocking the other. Therefore, block the ^{7}Li light and place a mirror along its line of sight, the inside middle of the heat pipe should now be visible. Change the current of the laser until you see a faint glow of red, dial the grating to increase the brightness. Check that this is the ^{6}Li saturated absorption signal since we have both in the same heat pipe, if it is ^{7}Li, repeat.

Something that I (and everyone else on this experiment) have learned, our experiment is very sensitive to the alignment of the optical pumping which can lead to poor lifetimes and low atom numbers in the MT. We recently reduced the beam waist of the optical pumping to increase the effectiveness, but the alignment of the optical pumping beams must still be well balanced in power and angle (the beams cross by about 3 degrees). If the MT is not evaporating well, almost every time the

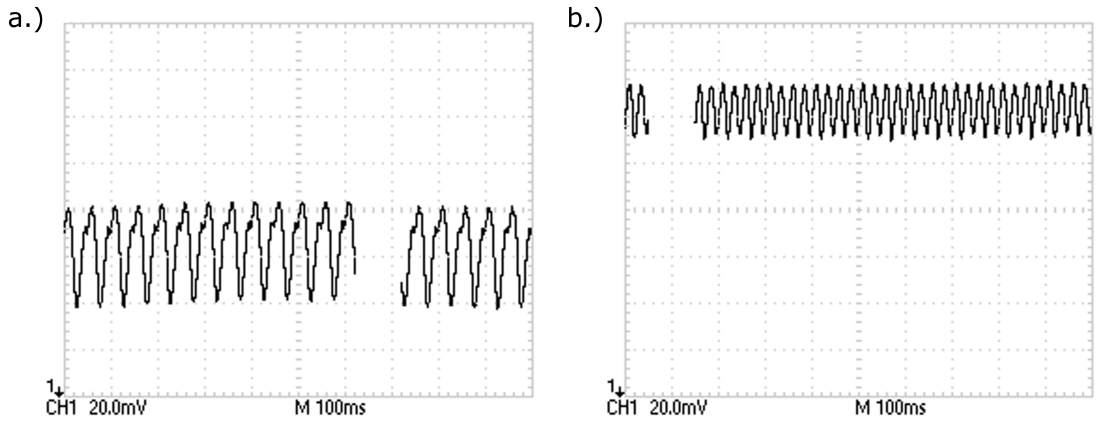

Figure 6.1 : The below threshold (60 mA) injection power of S6 while scanning the control voltage on the VCO of the offset AOM. We are scanning with a triangle wave of amplitude 0.2 V at 20 Hz. (a.) A scope trace of S6 when poorly injected (note the large amplitude of the signal), the average power is 2.7 mW. (b.) A scope trace of S6 when well injected on the same scale and offset with an average power of 2.9 mW. S7 shows the same features just at a different average value.

cause is insufficient optical pumping, in this case, check the alignment and power in the optical pumping path. This should not change, however, unless the MOT has been realigned or the MT coils have been removed.

To inject S6 and S7 such that they scan during the experiment without coming unlocked, optimize the injection while scanning the control voltage. The total power should only decrease by a couple percent from steady state injection, but the power should be as flat as possible (see Fig. 6.1).

6.2 Future Improvements

While our optics and locks for the red laser system are finally stable, the IR is falling behind. Soon we plan to replace or rebuild the AOM controller for the single-beam trap such that the RF power is constant with frequency. This should help stabilize the pointing of the beam. The lattice beam AOM drivers should also be updated to be more robust.

An improvement that will occur at the next oven change is adding an additional

heater at the front of the nozzle, this will make the oven wrapping procedure slightly different from Partridge's Ph.D. thesis [2]. Last year there were a few mishaps with the oven in the lab. We have found that we can not easily unclog our nozzle without the back of the oven increasing beyond 600°C, which is the temperature that the fiberglass insulation begins to break down. By wrapping just the front of the nozzle, when it clogs we will turn on this heater allowing the nozzle gradient to be canceled and the entire oven to heat to near 600°C to clear any clogs.

The laser system is not in a final state either. These improvements have been modified slightly since their first installation and will continue to be adjusted in cases where we can increase stability. Removing S1 and moving the frequency reference of M3 is likely. Also, room has been cleared on the imaging side of the table for shortening the beam path to the ^{6}Li MOT fiber.

6.3 Experimental Progress

Now that the laser system is stable and the majority of our improvements are finished, we are working continuously towards our experimental goals mentioned in Sec. 1.1. The 1D phase diagram introduced two interesting phenomena that we are attempting to explore; the inversion of the phases between 1D and 3D and the identification of the partially-polarized phase that occupies the majority of the phase diagram. I will briefly discuss how we intend to study these phenomena.

6.3.1 Probing the 1D-3D Crossover

We intend to map the phase diagram in the crossover regime at different lattice depths. This is possible on the experiment by use of liquid crystal retarders (LCRs). By varying a voltage to the LCR, we can change from a 3D trap to a lattice configuration during an experimental sequence. These allow us to vary the strength of the lattice

on sequential experiments by rotating the polarization of the retro-reflected lattice beam. By varying the spin-imbalance at constant lattice depths between 2 times the recoil energy (E_r) to 8 E_r we will have full phase diagrams at a range of lattice depths in the crossover regime. These diagrams should give a clear picture of how the cloud exhibits 1D and 3D structure.

6.3.2 The Search for Proof of FFLO

Theory implies that the partially-polarized phase in the 1D phase diagram is the FFLO superfluid phase. We will attempt to prove the existence of this phase by showing that the atoms are pairing with a non-zero center of mass momentum. The best method is by measuring the pair momentum distribution in 1D. This can be accomplished by canceling the harmonic confinement along the axial direction of the tube. As mentioned in Sec. 1.2, the lattice works via the AC Stark shift. The trap is red detuned from resonance which causes the atoms to be attracted to the light. By using a laser that is blue detuned in the same plane as the lattice beams, the potential will be positive and the atoms will be repelled, shown in Fig. 6.3.2. We have chosen 532 nm because we can supply sufficient power at that detuning. By matching the beam waists of the lattice and the anti-confinement laser, the two potentials will cancel. For a 12 E_r lattice, about 5.4W of 532 nm light will be necessary. This will leave the tubes of the lattice intact but allow free expansion of the atoms. After allowing the atoms to expand for a few milliseconds (this time will need adjustment as we begin the experiment), the momentum distribution shown in Fig. 1.4 should become visible.

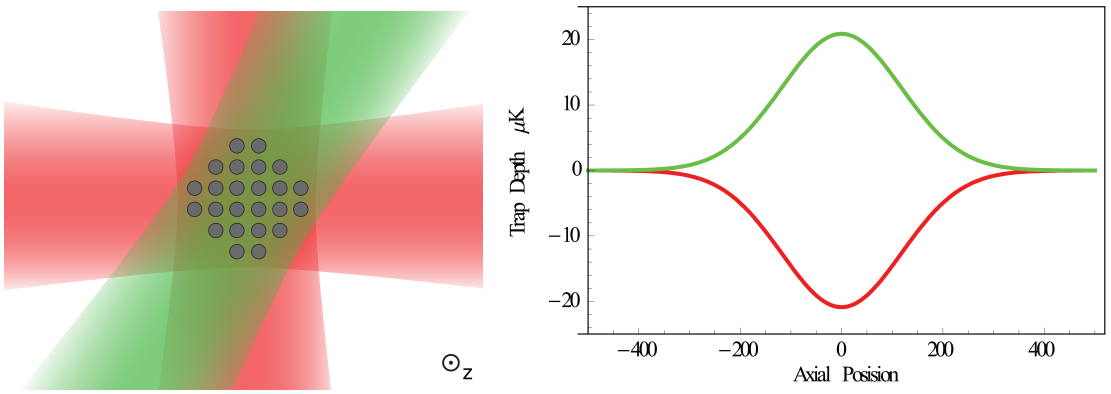

Figure 6.2 : The experimental implementation of the anti-confinement beam. (left) The beam is 60 degrees away from one of the lattice beams (30 degrees from the other) but still within the plane of the lattice beams and perpendicular to the z-axis. (right) Trap depth in μK along axial direction of the central tube of the lattice. The potentials for (red) the IR lattice and (green) the anti-trapping beam. This assumes the two traps have the same beam waist, with 1.4 W per beam in the lattice and 5.4 W of 532 nm anti-trapping light.

Appendix A

Experimental Benchmarks

I have included a table of all the red diode lasers currently on the laser table and their operating powers (Table A.1). This is useful in case a diode begins to fail. We have noticed an interesting failure mode on this experiment where the output power of the diode remains relatively constant but the below threshold injection power drops and the slave laser is no longer able to be injected. This has happened for 2 of our older diodes in slave lasers in the last year, as compared to a typical failure mode where the output power drops and the threshold current changes.

By monitoring all the powers on the table and keeping note of what is changing it is easier to pinpoint where problems occur. Most of the time problems start with low power or a poorly locked laser.

Other important factors to keep an eye on, especially for good evaporation in the MT, are the temperatures and atom number at each stage of the experiment. We have started the good habit of taking these measurements daily and keeping a log. In general, certain benchmarks much be met to guarantee the atoms evaporate (Table A.2).

Laser	P_{Typ}	P_{bt}	Diode
^{6}Li Power Amp Slave (S1)	9 mW	0.9 mW	Phillips 10 mW
^{6}Li Repump Slave (S2)	27 mW	2.6 mW	Hitachi HL6555G
^{6}Li TA seed Slave (S3)	45 mW	4.8 mW	Hitachi HL6555G
^{6}Li Zeeman Slave (S4)	27 mW	0.25 mW	Mitsubishi ML101J8
^{6}Li Imaging Slave (S9)	50 mW	7 mW	Hitachi HL6555G
^{7}Li Power Amp Slave (S5)	50 mW	2.1 mW	Hitachi HL6555G
^{7}Li Trap Slave (S6)	50 mW	3.2 mW	Hitachi HL6555G
^{7}Li Repump Slave (S7)	50 mW	2.3 mW	Hitachi HL6555G
^{7}Li Zeeman Slave (S8)	45 mW	4.1 mW	Hitachi HL6555G
^{6}Li Heat pipe Master(M1)	20 mW	NA	Hitachi HL6555G
^{6}Li Repump Master (M2)	10 mW	NA	Hitachi HL6555G
^{6}Li Imaging Master(M3)	18 mW	NA	Hitachi HL6555G
^{7}Li Heat pipe Master (DL Pro)	19 mW	NA	Toptica

Table A.1 : A list of each laser and its typical output power (P_{Typ}) for a current of $\sim$130 mA measured directly after the isolator. When the power out of the laser begins to drop, that is a sign the diode is ageing and may need to be replaced. The below threshold power (P_{bt}) is measured at a current of 60 mA for all the slaves except S1 which is measured at 27 mA. This is also measured directly after the isolator when the slave injection is well aligned and the seed laser is locked. Not reaching P_{bt} typically means the alignment is not optimum. The name in parenthesis is how the lasers are commonly referred to in the lab.

	Atom Number ($\times 10^9$)	Temperature (μK)
^{7}Li MOT	18.0	900
^{7}Li cMOT	16.5	600
^{6}Li MOT	2.4	-
^{7}Li MT 1 s holding	5.0	500
^{7}Li MT 45 s evaporation	0.17	42.0
^{6}Li MT 1 s holding	0.25	-

Table A.2 : All of the benchmark temperatures have been taken with ^{7}Li because it is doing the active cooling for the majority of evaporation. The important factor for ^{6}Li is that enough atoms are loaded into the MT. For ^{7}Li, all of the atom numbers were calculated from fluorescence images using 0γ detuning, 2 ms time of flight expansion, and 100 μs pulse time for the MOT beams. The ^{6}Li atom numbers were also obtained from fluorescence images using $\sim 5\gamma$ detuning, 2 ms time of flight expansion, and a pulse time of 300 μs. The number was calculated from the images according to the method described in Sec. 5.1.2. The MOT fluorescence images are taken after the Zeeman slower shutter has closed but before any cooling and compression processes have started. The cMOT fluorescence images are taken once the compression ramps described in Sec. 3.2 are completed and before optical pumping. MT 1 s holding means we load into the MT, hold the atoms and do not evaporate for 1 s, then take the fluorescence image. Finally, the ^{7}Li 45 s evaporation is loading into the MT without any ^{6}Li and following the normal RF evaporation, but stopping at 45 s for a fluorescence image. The temperatures are determined by taking a time of flight sequence from 1-3.5 ms at each of these points and following the procedure described in Sec. 5.1.2.

Bibliography

[1] K. E. Strecker, *Sympathetic Cooling of a Bose/Fermi Mixture of Lithium to Quantum Degeneracy.* Master's thesis, Rice University, 2002.

[2] G. B. Partridge, *Paring of Fermionic ^{6}Li Throughout the BEC-BCS Crossover.* PhD thesis, Rice University, 2007.

[3] Y. A. Liao, *Strongly Interacting Fermi Gases in 3D and 1D.* PhD thesis, Rice University, 2011.

[4] Y. A. Liao, A. S. C. Rittner, T. Paprotta, W. Li, G. B. Partridge, R. G. Hulet, S. K. Baur, and E. J. Mueller, "Spin-imbalance in a one-dimensional Fermi gas." *Nature*, **467** 567 (2010).

[5] K. E. Strecker, *Tunable Interaction in Quantum Degenerate Lithium.* PhD thesis, Rice University, 2004.

[6] G. B. Partridge, K. E. Strecker, R. I. Kamar, M. Jack, and R. G. Hulet, "Molecular Probe of Pairing in the BEC-BCS Crossover." *Phys. Rev. Lett.*, **95** 020404 (2005).

[7] G. B. Partridge, W. Li, R. I. Kamar, Y. A. Liao, and R. G. Hulet, "Pairing and Phase Separation in a Polarized Fermi Gas." *Science*, **311** 503 (2006).

[8] Y. A. Liao, M. Revelle, T. Paprotta, A. S. C. Rittner, W. Li, G. B. Partridge, and R. G. Hulet, "Metastability in Spin-Polarized Fermi Gases." *Phys. Rev. Lett.*, **107** 145305 (2011).

[9] M. M. Parish and D. A. Huse, "Evaporative depolarization and spin transport in a unitary trapped Fermi gas." *Phys. Rev. A*, **80** 063605 (2009).

[10] G. Orso, "Attractive Fermi Gases with Unequal Spin Populations in Highly Elongated Traps." *Phys. Rev. Lett.*, **98** 070402 (2007).

[11] L. Radzihovsky and D. E. Sheehy, "Imbalanced Feshbach-resonant Fermi gases." *Rep. Prog. Phys.*, **73** 076501 (2010).

[12] M. M. Parish, S. K. Baur, E. J. Mueller, and D. A. Huse, "Quasi-one-dimensional polarized fermi superfluids." *Phys. Rev. Lett.*, **99** 250403 (2007).

[13] F. Chevy and C. Mora, "Ultra-cold polarized Fermi gases." *Rep. Prog. Phys.*, **73** 112401 (2010).

[14] Y. Shin, M. W. Zwierlein, C. H. Schunck, A. Schirotzek, and W. Ketterle, "Observation of Phase Separation in a Strongly Interacting Imbalanced Fermi Gas." *Phys. Rev. Lett.*, **97** 030401 (2006).

[15] P. Fulde and R. A. Ferrell, "Superconductivity in a strong spin-exchange field." *Phys. Rev.*, **135** 3A (1964).

[16] A. I. Larkin and Y. N. Ovchinnikov, "Inhomogeneous state of superconductors." *JETP*, **47** 1136 (1964).

[17] M. R. Bakhtiari, M. J. Leskinen, and P. Törmä, "Spectral Signatures of the Fulde-Ferrell-Larkin-Ovchinnikov Order Parameter in One-Dimensional Optical Lattices." *Phys. Rev. Lett.*, **101** 120404 (2008).

[18] M. Swanson, Y. L. Loh, and N. Trivedi, "Proposal for interferometric detection of the topological character of modulated superfluidity in ultracold Fermi gases." *New J. Phys.*, **14** 033036 (2012).

[19] R. M. Lutchyn, M. Dzero, and V. M. Yakovenko, "Spectroscopy of the soliton lattice formation in quasi-one-dimensional fermionic superfluids with population

imbalance." *Phys. Rev. A*, **84** 033609 (2011).

[20] D. E. Sheehy and L. Radzihovsky, "BEC-BCS crossover, phase transitions and phase separation in polarized resonantly-paired superuids." *Ann. of Phys.*, **322** 1790 (2008).

[21] M. Rizzi, M. Polini, M. A. Cazalilla, M. R. Bakhtiari, M. P. Tosi, and R. Fazio, "Fulde-Ferrell-Larkin-Ovchinnikov pairing in one-dimensional optical lattices." *Phys. Rev. B*, **77** 245105 (2008).

[22] M. Casula, D. M. Ceperley, and E. J. Mueller, "Quantum Monte Carlo study of one-dimensional trapped fermions with attractive contact interactions." *Phys. Rev. A*, **78** 033607 (2008).

[23] C. J. Bolech, F. Heidrich-Meisner, S. Langer, I. P. McCulloch, G. Orso, and M. Rigol, "Long-Time Behavior of the Momentum Distribution During the Sudden Expansion of a Spin-Imbalanced Fermi Gas in One Dimension." *Phys. Rev. Lett.*, **109** 110602 (2012).

[24] G. B. Partridge, *An Improved System for Creating Ultracold Fermi Gases of* ^{6}*Li.* Master's thesis, Rice University, 2003.

[25] C. J. Welford, *Systems for the Radiative Trapping of Lithium and the Tuning of its Interactions via Magnetic Field Control.* Master's thesis, Rice University, 2007.

[26] C. A. Sackett, C. C. Bradley, and R. G. Hulet, "Optimization of evaporative cooling." *Phys. Rev. A*, **55** 3797 (1997).

[27] W. Ketterle and M. W. Zwierlein, "Making, probing and understanding ultracold Fermi gases." *Rivista del Nuovo Cimento*, **31** 247 (2008).

[28] T. Paprotta, *A 2D Optical Lattice for Creating a 1D Fermi Gas*. Master's thesis, Rice University, 2009.

[29] C. J. Foot, *Atomic Physics*. Oxford, 2005.

[30] P. D. Lett, W. D. Phillips, S. L. Rolston, C. E. Tanner, R. N. Watts, and C. I. Westbrook, "Optical molasses." *J. Opt. Soc. Am. B*, **6** 11, 2084 (1989).

[31] K. G. Libbrecht and J. Hall, "A low-noise high-speed diode laser current controller." *Rev. Sci. Instrum.*, **64** 8 (1993).

[32] Basler Vision Technologies, *User's Manual for GigE Vision Cameras*, 05 ed., June 2007.

[33] W. I. McAlexander, *Collisional Interactions in an Ultracold Lithium Gas*. PhD thesis, Rice University, 2000.

[34] G. Ritt, G. Cennini, C. Geckeler, and M. Weitz, "Laser frequency offset locking using a side of filter technique." *Appl. Phys. B*, **79** 363 (2005).